Journal of the Franklin Institute 361 (2024) 106854

Contents lists available at ScienceDirect

Journal of the Franklin Institute

journal homepage: www.elsevier.com/locate/fi

Adaptive control for hybrid dynamical systems with user-defined rate of convergence

Mattia Gramuglia [a], Giri M. Kumar [a], Andrea L'Afflitto [b,*]

[a] *Department of Mechanical Engineering, Virginia Tech, Blacksburg, VA 24061, USA*
[b] *Grado Department of Industrial and Systems Engineering, Virginia Tech, Blacksburg, VA 24061, USA*

ARTICLE INFO

Keywords:
Hybrid dynamical systems
Two-layer model reference adaptive control
Fast convergence

ABSTRACT

This paper presents a model reference adaptive control (MRAC) system for nonlinear, time-varying, hybrid dynamical plants affected by modeling uncertainties. This system is unique because, in addition to regulating the trajectory tracking error to zero, it allows the user to set the rate of convergence of the tracking error between consecutive resetting events. This proposed result has been possible by leveraging an auxiliary trajectory tracking error dynamics to accelerate convergence of the trajectory tracking error according to the two-layer MRAC framework. The resetting logic of both the reference model and the auxiliary trajectory tracking error dynamics bound variations in the trajectory tracking error due to undesired resetting events in the plant dynamics. The resetting events of the reference and auxiliary model also reduce the trajectory tracking error whenever some dwell-time condition is met. Finally, the resetting logic of both the reference model and the auxiliary trajectory tracking error reduces the control effort at isolated time-instants. Three numerical examples demonstrate the applicability of the proposed result as well as their advantages over alternative adaptive control techniques for nonlinear, time-varying, hybrid dynamical plants as well as classical MRAC.

1. Introduction

1.1. Motivation

In control systems theory, a very common assumption in the modeling of dynamical plants is their continuity in time and Lipschitz continuity in the state since these conditions assure the existence and uniqueness of solutions to ordinary differential equations [1, Ch. 3]. Although these assumptions are sufficiently accurate to model many problems of practical interest, the problem of controlling plant models that are best captured under weaker assumptions, such as mixed discrete-time and continuous-time dynamics, is rapidly gaining more interest among researchers and practitioners in control theory. For instance, there is a considerably growing number of problems that involve discrete-time decision variables that can be selected at unknown time instants [2]. Furthermore, there is growing attention to problems involving the integration of continuous-time and discrete-time systems. For instance, in autonomous robotic systems, such as cars or autonomous aircraft, high-level planning systems usually operate at a lower rate than low-level control systems, and, for this reason, the former are can be considered discrete-time systems and the latter as continuous-time systems [3]. Finally, there is an emerging interest in mechanical systems subject to contact forces and other phenomena, such as friction, which experience instantaneous variations in the state or the plant model, or impulsive forces and torques. For these reasons, the need for control systems for hybrid plants, that is, plants captured by sets of differential and difference equations, and subject

* Corresponding author.
E-mail addresses: mgramuglia@vt.edu (M. Gramuglia), girimugundan@vt.edu (G.M. Kumar), a.lafflitto@vt.edu (A. L'Afflitto).

https://doi.org/10.1016/j.jfranklin.2024.106854
Received 14 July 2023; Received in revised form 16 March 2024; Accepted 16 April 2024
Available online 19 April 2024

to instantaneous variations in the state, the system parameters, the plant mode, and external disturbances is becoming increasingly compelling. In problems of practical interest, however, modeling uncertainties are unavoidable, and, hence, the need for adaptive control systems, such as model reference adaptive control (MRAC) systems, for hybrid plants has become a necessity.

1.2. Summary of results

In [4], the classical LaSalle–Yoshizawa theorem [5, Th. 4.7] has been extended for the first time to nonlinear time-varying hybrid (NTVH) dynamical systems. These extensions included both complete and not complete solutions converging to a closed and bounded subset of the state space [6, Ch. 3]. An application of this result has been the design of the first MRAC system for NTVH plants affected by parametric and matched uncertainties, whose reset dynamics are unknown.

Despite its classical counterpart [7, Ch. 9], two-layer MRAC [8] allows the user to explicitly set the rate of convergence of the trajectory tracking error during the transient phase. This result is attained by introducing an auxiliary reference model that drives the controlled plant's trajectory to the reference trajectory before the reference model's transient dynamics have decayed. Indeed, a key problem of classical MRAC lies in the fact that the trajectory of the closed-loop plant converges to the reference trajectory after the transient dynamics of the reference model have decayed. This fact limits the effectiveness of classical MRAC since the transient stage is highly critical in most problems of practical interest, and it is desirable that the controlled plant mimics the reference model as closely as possible. As discussed in [8], several solutions were devised to guarantee user-defined rates of convergence of the closed-loop trajectory tracking error dynamics. However, these solutions require modifying the reference model [9], which limit the user's ability to set the reference model arbitrarily, involve barrier functions [10], which usually imply overly aggressive control inputs, or require the use of estimators [11], which add further complexity to the system. Instead, for its close resemblance to MRAC, the fact that the reference model is not modified, barrier Lyapunov functions are not employed, and no estimator is needed, two-layer MRAC appears to be a faster, and less demanding solution to the problem of regulating unknown, nonlinear dynamical models, while setting explicitly the closed-loop system's rate of convergence.

In this paper, we merge the results presented in [4,8] and present an MRAC architecture for NTVH plants affected by matched uncertainties, parametric uncertainties, and uncertainties in the resetting events of the plant. A unique feature of the proposed architecture is that it allows steering the closed-loop trajectory to the reference model's trajectory uniformly in the sequence of resetting times and imposing a user-defined rate of convergence on the closed-loop system. The rate of convergence is set by tuning the eigenvalues of the auxiliary reference model; this result is unprecedented in the context of hybrid systems theory. Furthermore, the proposed control architecture allows for resetting events in both the reference and the auxiliary model that reduce the trajectory tracking error introduced by undesired resetting events in the plant dynamics, which occur at time instants that are unknown in advance. Additionally, the proposed control architecture is unique for its ability to instantaneously reduce the trajectory tracking error to zero on isolated instances, and hence, instantaneously reduce the control effort, without altering the closed-loop system's overall performance.

The proposed control architecture distinguishes itself for several additional features. Firstly, the control law resembles the one of classical and two-layer MRAC, which eases its implementation. The proposed control law is the product of an adaptive gain matrix and a vector function of the state, the reference command input, the regressor vector, and the trajectory tracking error. Secondly, the adaptive gain matrix is computed as an absolutely continuous solution of an adaptive law that is similar to the adaptive law of classical two-layer MRAC. Finally, instead of the trajectory tracking error, the adaptive law involves an auxiliary error state. This auxiliary error state captures the difference between the trajectory tracking error, that is, the difference between the controlled plant state and the reference model's state, and an auxiliary trajectory tracking error. The auxiliary trajectory tracking error is the state of a user-defined, time-invariant, hybrid, uncontrolled, linear system. For each mode of this auxiliary system, the eigenvalues of the state matrix are smaller than any eigenvalue of the state matrix characterizing the reference model. The role of the auxiliary trajectory tracking error is to steer the controlled plant trajectory to zero at a rate faster than the rate of convergence of the reference model.

1.3. Literature review and relevance of the proposed results

In 2022, the authors of [12] remarked on how the adaptive control problem for hybrid dynamical systems is substantially under-explored. Among existing results on the adaptive control of hybrid dynamical systems, it is worthwhile recalling [13], where the authors consider time-invariant dynamical systems and require the user to provide a Lyapunov-like function to design an adaptive system. In [14], the authors proposed an adaptive system for the parameter estimation of linear, hybrid systems with matched uncertainties. An adaptive control system for linear, single-input single-output hybrid plants was proposed in [15], and a linear hybrid adaptive control method for a class of discrete-time multi-input multi-output systems was proposed in [16]. Worthy of mention are also the robust and adaptive systems for linear, time-varying, stochastic hybrid plants recently presented in [17,18]. A more conspicuous body of literature concerns the problem of designing adaptive control systems for switched plants. Switched plants are a subclass of hybrid plants since they experience instantaneous changes in the plant dynamics, but whose trajectories are continuous in time. Among these works, we recall [12,19–23] to name a few.

This paper advances the state of the art because the proposed MRAC system applies to nonlinear, time-varying, multi-input multi-state plants. Furthermore, the proposed results apply to hybrid plants, and not switched plants only. The proposed MRAC system applies to plants affected by functional and parametric uncertainties. Additionally, this work does not require the user to define the Lyapunov function to certify the effectiveness of the control system, which is usually a daunting task. Finally, this paper addresses the convergence problem in controlled NTVH plants, which is unprecedented. Worthy of remark is that, to the authors' knowledge, together with [4], this is the only work on MRAC systems for nonlinear, time-varying, hybrid plants.

1.4. Content outline

This paper is structured as follows. In Section 2, we present the essential notation used throughout this work. In Section 3, we recall key notions of hybrid systems theory needed to develop the proposed control system. In Section 4, we introduce the notion of rate of convergence for linear, time-invariant, hybrid plants, and provide estimates on the rate of convergence of these systems. In Section 5, we present the proposed MRAC system for NTVH plants. In Section 6, we discuss three numerical examples that highlight both the applicability of the proposed control architecture and its advantages over the results shown in [4] and classical MRAC [7, Ch. 9]. The first of these examples involves the outer loop dynamics of a quad-biplane unmanned aerial vehicle (UAV). A quad-biplane is equipped with two wings and four propellers so that it can operate either as a fixed-wing aircraft or as a quadcopter according to needs. Since the dynamics of this vehicle change substantially and rapidly across the two modes of operation, an NTVH model is most suitable for an accurate mathematical representation. The second example involves an actuated disk tasked with following some user-defined trajectory throughout a maze. This trajectory is unfeasible both because it requires instantaneous changes in the disk's translational velocity, and because it would require the disk to penetrate the walls of the maze. To further challenge the proposed control architecture, collisions between the disk and the walls are modeled as purely elastic and, hence, introduce resetting events into the plant. The final example shows the applicability and the advantages of the proposed control system when applied to a multi-rotor UAV tasked with transporting an unknown, unsteady payload while traveling at high speeds along a lemniscate trajectory. Since the UAV experiences large rotations to closely follow this aggressive trajectory, the payload, whose inertial properties and location in the casing are unknown, impacts the vehicle are well captured by an NTVH model. Finally, in Section 7, we draw conclusions and outline future work directions. The Appendix summarized essential elements of two-layer MRAC for continuous-time plants [8].

2. Notation

The *set of positive integers* is designated by $\mathbb{N}$, the *set of nonnegative integers* is designated by $\overline{\mathbb{N}}$, *set of real numbers* is represented by $\mathbb{R}$, *set of negative real numbers* is represented by $\mathbb{R}_-$, the *set of* $n\times 1$ *real column vectors* is indicated by $\mathbb{R}^n$, and the *set of* $n\times m$ *real matrices* is indicated by $\mathbb{R}^{n\times m}$. The *boundary of* $\mathcal{R}\subset\mathbb{R}^n$ is denoted by $\partial\mathcal{R}$, and the *closure of* $\mathcal{R}$ is denoted by $\overline{\mathcal{R}}$. The *open ball of radius* $\rho>0$ *centered at* $x\in\mathbb{R}^n$ is denoted by $\mathcal{B}_\rho(x)$.

The *zero vector* in $\mathbb{R}^n$ and the *zero matrix* in $\mathbb{R}^{n\times m}$ are denoted by 0_n and $0_{n\times m}$, respectively, and the *identity matrix* in $\mathbb{R}^{n\times n}$ is denoted by $\mathbf{1}_n$. The *Euclidean vector norm* and its *equi-induced matrix norm* are denoted by $\|\cdot\|$ [24, Def. 9.4.1]. The eigenvalues of $A\in\mathbb{R}^{n\times n}$ with largest and smallest real part are denoted by $\lambda_{\max}(A)$ and $\lambda_{\min}(A)$, respectively. Given the set of matrices $\{Q_\sigma\}_{\sigma\in\Sigma}$, where Σ contains finitely many elements, let $\bar{\lambda}_{\min}\left(\{Q_\sigma\}_{\sigma\in\Sigma}\right)\triangleq\min\{\lambda_{\min}\left(Q_\sigma\right),\ \sigma\in\Sigma\}$ and $\bar{\lambda}_{\max}\left(\{Q_\sigma\}_{\sigma\in\Sigma}\right)\triangleq\min\{\lambda_{\max}\left(Q_\sigma\right),\ \sigma\in\Sigma\}$ denote the eigenvalues of the collection of matrices $\{Q_\sigma\}_{\sigma\in\Sigma}$ with smallest and largest real parts, respectively.

3. Fundamentals of hybrid systems theory

Time-varying, hybrid dynamical systems can be captured by

$$\dot{x}(t)=f_{\rm c}(t,x(t)),\qquad (t,x(t))\notin\mathcal{R},\tag{1}$$

$$x(t^+)=g_{\rm d}(t,x(t)),\qquad (t,x(t))\in\mathcal{R},\tag{2}$$

with $x(t_0)=x_0$ and initial time $t_0\in[0,\infty)$, $\mathcal{Z}\subseteq\mathbb{R}^n$ an open set such that $0\in\mathcal{Z}$, and $\mathcal{R}\subset(t_0,\infty)\times\mathcal{Z}$. The *flow map*, $f_{\rm c}:[t_0,\infty)\times\mathcal{Z}\to\mathbb{R}^n$ is Lebesgue integrable, locally bounded, and such that $f_{\rm c}(t,0_n)=0_n$ for all $t\in[t_0,\infty)$. The *jump map* $g_{\rm d}:[t_0,\infty)\times\mathcal{Z}\to\mathbb{R}^n$ is continuous and locally bounded. A *resetting event* occurs whenever $(t,x(t))\in\mathcal{R}$ for some $t\geq t_0$. The *resetting time before* $t\geq t_0$ is defined as $t_k\triangleq\min\{t\geq t_{k-1}:(t,s(t,t_{k-1},x_{k-1}))\notin\mathcal{R}\}$ for all $k\in\mathbb{N}$, where $s:[t_0,\infty)\times[0,\infty)\times\mathcal{Z}\to\mathcal{Z}$ denotes the *flow* of solutions of (1) and (2). The system (1) and (2) is assumed to be *left-continuous* [25, Def. 12.1]; the proposed arguments can be ported to right-continuous systems [26]. We also assume that $(t_0,x_0)\notin\mathcal{R}$, and the case $(t_0,x_0)\in\mathcal{R}$ can be addressed applying similar arguments.

Definition 3.1. Let $\mathcal{I}\subseteq[t_0,\infty)$ be connected and such that $t_0\in\mathcal{I}$. Let $x:\mathcal{I}\to\mathcal{Z}$ be piecewise absolutely continuous, have a finite number of discontinuities on any compact subinterval of $\mathcal{I}$, and be such that

$$\dot{x}(t)\in K[f_{\rm c}](t,x(t)),\qquad \text{for all } (t,x(t))\in\overline{\mathcal{T}},\tag{3}$$

$$x(t^+)\in K[g_{\rm d}](t,x(t)),\qquad \text{for all } (t,x(t))\in\overline{\mathcal{R}},\tag{4}$$

where $\mathcal{T}\triangleq(\mathcal{I}\times\mathcal{Z})\setminus\mathcal{R}$,

$$K[f_{\rm c}](t,x)\triangleq\bigcap_{\delta>0}\overline{\rm co}\left(f_{\rm c}\left(\overline{\mathcal{B}}_\delta\left(\begin{bmatrix}t\\x\end{bmatrix}\right)\cap\mathcal{T}\right)\right),\quad (t,x)\in\overline{\mathcal{T}},\tag{5}$$

$$K[g_{\rm d}](t,x)\triangleq\bigcap_{\delta>0}\overline{g_{\rm d}\left(\overline{\mathcal{B}}_\delta\left(\begin{bmatrix}t\\x\end{bmatrix}\right)\cap\mathcal{R}\right)},\quad (t,x)\in\overline{\mathcal{R}},\tag{6}$$

denote the *Krasovskii regularizations of* (1) and (2), respectively, and $\overline{\rm co}(\cdot)$ denotes the convex closure of its argument. Then, $x(\cdot)$ is a *Krasovskii solution of* (1) and (2). If there do not exist a connected set $\mathcal{J}\subseteq[t_0,\infty)$ and a Krasovskii solution $\overline{x}:\mathcal{J}\to\mathcal{Z}$ of (1) and (2) such that $\mathcal{I}\subset\mathcal{J}$ and $\overline{x}(t)=x(t)$, $t\in\mathcal{I}$, then $x:\mathcal{I}\to\mathcal{Z}$ is a *maximal Krasovskii solution* of (1) and (2). If $\mathcal{I}=[t_0,\infty)$, then a Krasovskii solution $x:\mathcal{I}\to\mathcal{Z}$ of (1) and (2) is *complete*.

Discontinuities of solutions of (1) and (2) in the sense of Krasovskii are assumed to occur at the resetting times only. Furthermore, we make the following assumptions.

Assumption 3.1. If $(t, x(t)) \in \overline{\mathcal{R}} \setminus \mathcal{R}$, then there exists $\varepsilon > 0$ such that, for all $\delta \in (0, \varepsilon)$, $s(t+\delta, t, x(t)) \notin \mathcal{R}$.

Assumption 3.2. If $(t_k, x(t_k)) \in \partial\mathcal{R} \cap \mathcal{R}$, then there exists $\varepsilon > 0$ such that, for all $\delta \in (0, \varepsilon)$, $s(t_k+\delta, t_k, x(t_k^+)) \notin \mathcal{R}$.

By Assumptions 3.1 and 3.2, solutions of (1) and (2) do not enter the interior of $\mathcal{R}$. Furthermore, by Assumption 3.2, the phenomenon of beating is averted, that is, solutions to not incur into the same resetting event multiple times in zero time.

Next, we present two generalizations of the LaSalle–Yoshizawa theorem to the NTVH dynamical system (1) and (2). These results prove sufficient conditions for pre-attractivity for (1) and (2) of a compact set containing the origin. To state these results, let $x : [t_0, \infty) \to \mathcal{Z}$ be a solution of (1) and (2). Furthermore, let $V : [t_0, \infty) \times \mathcal{Z} \to \mathbb{R}$ be absolutely continuous over compact intervals of $[t_0, \infty)$ not containing resetting times in their interior for each $x \in \mathcal{Z}$, and, for each $t \in [t_0, \infty)$, Lipschitz continuous and regular over $\mathcal{Z}$ [27, pp. 63–64], [28, p. 39]. Let $W : \mathcal{Z} \to \mathbb{R}$ be absolutely continuous and nonnegative definite. Let $\bar{t}_k \in [t_0, \infty)$, $k \in \overline{\mathbb{N}}$, be such that $\bar{t}_0 = t_0$; $\bar{t}_1 = t_1$; if $\sum_{j=1}^{k-1} \left[V(t_j^+, x(t_j^+)) - V(t_j, x(t_j))\right] > 0$, $k \in \mathbb{N} \setminus \{1\}$, along a solution of (1) and (2), then

$$\bar{t}_k = \inf \left\{ t \in [t_0, \infty) : \int_{t_0}^{t} W(x(\tau))\mathrm{d}\tau \geq \sum_{j=1}^{k-1} \left[V(t_j^+, x(t_j^+)) - V(t_j, x(t_j))\right] \right\}; \tag{7}$$

and if $\sum_{j=1}^{k-1} \left[V(t_j^+, x(t_j^+)) - V(t_j, x(t_j))\right] \leq 0$, then $\bar{t}_k = t_1$. Finally, define the *critical times*

$$\hat{t}_k \triangleq \max\left\{t_k, \bar{t}_k\right\}. \tag{8}$$

Theorem 3.1 (*[4]*). *Consider the hybrid, time-varying, nonlinear dynamical system given by (1) and (2), assume that all solutions of (1) and (2) are complete, and assume that $\mathcal{Z} = \mathbb{R}^n$. Let $V : [t_0, \infty) \times \mathcal{Z} \to \mathbb{R}$ be absolutely continuous in its first argument over compact intervals of $[t_0, \infty) \subseteq \overline{\mathbb{R}}_+$ that do not contain resetting times in their interior for each $x \in \mathcal{Z}$ and Lipschitz continuous and regular in the second argument for each $t \in [t_0, \infty)$. Assume that*

$$W_1(x) \leq V(t, x) \leq W_2(x), \quad (t, x) \in [t_0, \infty) \times \mathcal{Z}, \tag{9}$$

$$\dot{V}(t, x) \leq -W(x), \quad (t, x) \notin \left([t_0, \infty) \times \left(\mathcal{Z} \setminus \overline{\mathcal{A}}\right)\right) \cap \mathcal{R}, \tag{10}$$

where $W_1, W_2 : \mathcal{Z} \to \mathbb{R}$ are positive-definite and radially unbounded, $\overline{\mathcal{A}} \subset \mathcal{Z}$ is compact and such that $0 \in \mathring{\mathcal{A}}$, and $W : \mathcal{Z} \to \mathbb{R}$ is continuously differentiable on $\mathcal{Z} \setminus \{0_n\}$, nonnegative-definite, and such that $W(x) > 0$ for all $x \in \mathcal{Z} \setminus \overline{\mathcal{A}}$. If

$$\hat{t}_k \leq t_k, \qquad k \in \overline{\mathbb{N}}, \tag{11}$$

and $\sum_{k=1}^{\infty} \left[V(t_k^+, x(t_k^+)) - V(t_k, x(t_k))\right]$ exists and is finite, then every maximal solution $x(\cdot)$ of (1) and (2) is uniformly bounded in $\{t_k\}_{k\in\overline{\mathbb{N}}}$ and such that $\lim_{t\to\infty} \operatorname{dist}(x(t), \overline{\mathcal{A}}) = 0$ for all $x_0 \in \mathbb{R}^n$ uniformly in $\{t_k\}_{k\in\overline{\mathbb{N}}}$.

A direct consequence of Theorem 3.1 is the following result, which provides sufficient conditions for the uniform boundedness and convergence of the solution of the NTVH system (1) and (2) to the origin.

Theorem 3.2. *Consider the NTVH dynamical system given by (1) and (2), assume that all maximal solutions of (1) and (2) are complete, and assume that $\mathcal{Z} = \mathbb{R}^n$. Let $V : [t_0, \infty) \times \mathcal{Z} \to \mathbb{R}$ be absolutely continuous in its first argument over compact intervals of $[t_0, \infty)$ that do not contain resetting times in their interior for each $x \in \mathcal{Z}$ and Lipschitz continuous and regular in the second argument for each $t \in [t_0, \infty)$. Assume that (9) is verified,*

$$\dot{V}(t, x) \leq -W(x), \qquad (t, x) \notin \left(\mathcal{R} \cup \left([t_0, \infty) \times \{0\}\right)\right), \tag{12}$$

where $W : \mathcal{Z} \to \mathbb{R}$ is continuously differentiable and nonnegative-definite, $\sum_{j=1}^{\infty} \left[V(t_j^+, x(t_j^+)) - V(t_j, x(t_j))\right]$ exists and is finite, and (11) is verified. Then, every maximal solution $x(\cdot)$ of (1) and (2) is uniformly bounded in $\{t_k\}_{k\in\overline{\mathbb{N}}}$ and such that $\lim_{t\to\infty} W(x(t)) = 0$ for all $x_0 \in \mathbb{R}^n$ uniformly $\{t_k\}_{k\in\overline{\mathbb{N}}}$.

Proof. The result follows from Theorem 3.2 with $\overline{\mathcal{A}} = \{0\}$. ■

4. Rate of convergence of linear hybrid dynamical systems

In this section, we introduce the notion of rate of convergence of linear, time-invariant, hybrid dynamical systems. Consider the linear, hybrid *dynamical system*

$$\begin{bmatrix}\dot{x}_{\mathrm{ref}}(t)\\ \dot{\sigma}(t)\end{bmatrix}=\begin{bmatrix}A_{\mathrm{ref},\sigma(t)}x_{\mathrm{ref}}(t)+B_{\mathrm{ref},\sigma(t)}u(t)\\ 0\end{bmatrix},\quad \begin{bmatrix}x_{\mathrm{ref}}(t_0)\\ \sigma(t_0)\end{bmatrix}=\begin{bmatrix}x_{\mathrm{ref},0}\\ \sigma_0\end{bmatrix},\quad (t,x_{\mathrm{ref}}(t))\notin\mathcal{R}_{\sigma(t)}, \tag{13}$$

$$\begin{bmatrix}x_{\mathrm{ref}}(t^+)\\ \sigma(t^+)\end{bmatrix}=g_{\mathrm{d},\sigma(t)}(t,x_{\mathrm{ref}}(t)),\qquad (t,x_{\mathrm{ref}}(t))\in\mathcal{R}_{\sigma(t)}, \tag{14}$$

where $x_{\mathrm{ref}}:[t_0,\infty)\to\mathbb{R}^n$, $\sigma:[t_0,\infty)\to\Sigma$, $\Sigma\triangleq\{1,\ldots,\sigma_{\max}\}$, $u:[t_0,\infty)\to\mathbb{R}^m$ is piecewise continuous and bounded, $A_{\mathrm{ref},\sigma}\in\mathbb{R}^{n\times n}$, $\sigma\in\Sigma$, is Hurwitz, $B_{\mathrm{ref},\sigma}\in\mathbb{R}^{n\times m}$, and $g_{\mathrm{d},\sigma}:[t_0,\infty)\times\mathcal{Z}\to\mathbb{R}^n$ is continuous in its arguments, locally bounded, and such that, together with the set of resetting events $\mathcal{R}\subset[t_0,\infty)\times(\mathcal{Z}\setminus\{0\})$, Assumptions 3.1 and 3.2 are verified.

By proceeding as in [6, Ch. 1], it can be proven that the linear, hybrid system (13) and (14) is a special case of (1) and (2). The mode $\sigma(\cdot)$ is a piecewise constant function used to track instantaneous variations in the continuous-time plant dynamics. Indeed, it follows from (13) that, between two consecutive resetting events, $\dot{\sigma}(t)=0$, and it follows from (14) that $\sigma(\cdot)$ varies only across resetting events.

Definition 4.1. Let $x_{\mathrm{ref}}:[t_0,\infty)\to\mathbb{R}^n$ denote a solution of (13) and (14) with $u(t)\equiv 0$, $t\ge t_0$. If $\lim_{t\to\infty}x_{\mathrm{ref}}(t)=0$ uniformly in $\{t_k\}_{k\in\overline{\mathbb{N}}}$, then the *rate of convergence of* $x_{\mathrm{ref}}(\cdot)$ is defined as

$$\alpha_{\max}(x_{\mathrm{ref}}(\cdot))\triangleq\sup_{x_{\mathrm{ref}}(t_0)\in\mathbb{R}^n\setminus\{0\}}\ \liminf_{t\to\infty}\frac{\log\|x_{\mathrm{ref}}(t)\|}{t_0-t}. \tag{15}$$

Definition 4.1 extends the classical definition of rate of convergence of continuous-time, linear, asymptotically stable dynamical systems [29]. The next result provides some properties of (13) and (14), which are essential to the scopes of this paper.

Lemma 4.1. *Consider the NTVH, linear dynamical system given by (13) and (14). Suppose that* $\lim_{t\to\infty}x_{\mathrm{ref}}(t)=0$ *uniformly in* $\{t_k\}_{k\in\overline{\mathbb{N}}}$ *with* $u(t)\equiv 0$, $t\ge t_0$. *Then,* $\alpha_{\max}(x_{\mathrm{ref}}(\cdot))=-\max_{\sigma\in\Sigma}\mathrm{Re}(\lambda_{\max}(A_{\mathrm{ref},\sigma}))$. *Furthermore, if* $u(\cdot)$ *is piecewise continuous and bounded, and Assumptions 3.1 and 3.2 are verified by (13) and (14), then there exist* $\xi_k:[t_0,\infty)\to\mathbb{R}_-$, $\gamma_1\ge 1$, *and* $\gamma_2\in(0,1)$ *such that, for any* $k\in\overline{\mathbb{N}}$,

$$\|x_{\mathrm{ref}}(t)\|\le g_{\mathrm{ub},k}(t)-\frac{\gamma_1}{\gamma_2}\max_{\sigma\in\Sigma}\frac{\|B_{\mathrm{ref},\sigma}\|}{\mathrm{Re}(\lambda_{\max}(A_{\mathrm{ref},\sigma}))}\sup_{t\in[t_0,\infty)}\|u(t)\|,\qquad t\in[t_k,t_{k+1}), \tag{16}$$

where

$$g_{\mathrm{ub},k}(t)\triangleq\gamma_1\|x_{\mathrm{ref}}(t_k^+)\|e^{\xi_k(t)(t-t_k)}+\max_{t\in[t_0,t_k)}g_{\mathrm{ub},k-1}(t),\qquad k\in\mathbb{N}, \tag{17}$$

$$g_{\mathrm{ub},0}(t)\triangleq\gamma_1\|x_{\mathrm{ref}}(t_0)\|e^{\xi_k(t)(t-t_0)}, \tag{18}$$

and $\liminf_{t\to\infty}\xi(t)=\max_{\sigma\in\Sigma}\mathrm{Re}(\lambda_{\max}(A_{\mathrm{ref},\sigma}))$.

Proof. It holds that $x_{\mathrm{ref}}(t)=e^{A_{\mathrm{ref},\sigma(t_k)}(t-t_k)}x_{\mathrm{ref}}(t_k^+)+\int_{t_k}^t e^{A_{\mathrm{ref},\sigma(\tau)}}B_{\mathrm{ref},\sigma(\tau)}u(\tau)\mathrm{d}\tau$, $t\in[t_k,t_{k+1})$, for all $k\in\overline{\mathbb{N}}$ [30, p. 33]. Thus, applying the triangle inequality and the Cauchy–Schwarz inequality, it holds that

$$\begin{aligned}\|x_{\mathrm{ref}}(t)\|&\le\|e^{A_{\mathrm{ref},\sigma(t_k)}(t-t_k)}\|\|x_{\mathrm{ref}}(t_k^+)\|\\&\quad+\|B_{\mathrm{ref},\sigma(t_k)}\|\sup_{t\in[t_k,t_{k+1})}\left(\|u(t)\|\int_{t_k}^t\left\|e^{A_{\mathrm{ref},\sigma(t)}(t-\tau)}\right\|\mathrm{d}\tau\right),\qquad t\in[t_k,t_{k+1}).\end{aligned} \tag{19}$$

As shown in [31], there exist $\xi:[t_0,\infty)\to\mathbb{R}_-$ and $\gamma_1\ge 1$ so that

$$\|e^{A_{\mathrm{ref},\sigma(t)}(t-t_k)}\|\le\gamma_1 e^{\xi(t)(t-t_k)},\qquad t\in[t_k,t_{k+1}), \tag{20}$$

where, if $\sigma(t)=\sigma(t_k)$ for all $t\ge t_k$, then $\lim_{t\to\infty}\xi(t)=\left[\mathrm{Re}(\lambda_{\max}(A_{\mathrm{ref},\sigma(t_k)}))\right]^+$. Hence, if $u(t)\equiv 0$, $t\ge t_0$, then it follows from (15) that $\alpha_{\max}(x_{\mathrm{ref}}(\cdot))=-\max_{\sigma\in\Sigma}\mathrm{Re}(\lambda_{\max}(A_{\mathrm{ref},\sigma}))$.

Since $\|I_n\|=1$, Fact 11.18.8 of [24] implies that $\|e^{A_{\mathrm{ref},\sigma}(t-\tau)}\|\le\gamma_1 e^{\gamma_2\mathrm{Re}(\lambda_{\max}(A_{\mathrm{ref},\sigma}))(t-\tau)}$, $\sigma\in\Sigma$, for all $t\in[t_0,\infty)$, for all $\tau\in[t_0,t]$, and for any $\gamma_2\in(0,1)$. Thus, (16) follows from (19) and the fact that, for any $k\in\overline{\mathbb{N}}$ and any $\sigma\in\Sigma$,

$$\begin{aligned}\int_{t_k}^t e^{\gamma_2\mathrm{Re}(\lambda_{\max}(A_{\mathrm{ref},\sigma}))(t-\tau)}\mathrm{d}\tau&\le\int_{t_k}^\infty e^{\gamma_2\mathrm{Re}(\lambda_{\max}(A_{\mathrm{ref},\sigma}))(t-\tau)}\mathrm{d}\tau\\&=-\left(\gamma_2\mathrm{Re}(\lambda_{\max}(A_{\mathrm{ref},\sigma}))\right)^{-1},\qquad t\in[t_k,t_{k+1}).\qquad\blacksquare\end{aligned}$$

5. Two-layer MRAC for hybrid systems

5.1. Plant and reference model dynamics

In this section, we present the two-layer MRAC law for NTVH plants affected by matched and parametric uncertainties, and uncertainties in the resetting events. To this goal, consider the *plant model*

$$\begin{bmatrix}\dot{x}(t)\\ \dot{\sigma}(t)\end{bmatrix} = \begin{bmatrix}A_{\sigma(t)}x(t) + B_{\sigma(t)}\left[u(t) + \tilde{\Theta}^{\mathrm{T}}_{\sigma(t)}\tilde{\Phi}_{\sigma(t)}(t, x(t))\right]\\ 0\end{bmatrix},$$
$$\begin{bmatrix}x(t_0)\\ \sigma(t_0)\end{bmatrix} = \begin{bmatrix}x_0\\ \sigma_0\end{bmatrix}, \qquad (t, x(t)) \notin \mathcal{R}_{\sigma(t)}, \tag{21}$$

$$\begin{bmatrix}x(t^+)\\ \sigma(t^+)\end{bmatrix} = g_{\mathrm{d},\sigma(t)}(t, x(t)), \qquad (t, x(t)) \in \mathcal{R}_{\sigma(t)}, \tag{22}$$

where $x : [t_0, \infty) \to \mathbb{R}^n$ denotes the *plant state*, the piecewise continuous function $u : [t_0, \infty) \to \mathbb{R}^m$ denotes the *control input*, $A_\sigma \in \mathbb{R}^{n\times n}$, $\sigma \in \Sigma$, is unknown, the mapping $\sigma \mapsto A_\sigma$ is unknown, the mapping $\sigma \mapsto B_\sigma$ is unknown, the pair (A_σ, B_σ) is controllable, $\tilde{\Theta}_\sigma \in \mathbb{R}^{\tilde{N}_\sigma\times m}$ is unknown, the mapping $\sigma \mapsto \tilde{\Theta}_\sigma$ is unknown, and the *regressor vector* $\tilde{\Phi}_\sigma : [t_0, \infty)\times\mathbb{R}^n \to \mathbb{R}^{\tilde{N}_\sigma}$ is Lipschitz continuous and known. The ith resetting time of the resetting event $\mathcal{R}_{\sigma_{i-1}}$, $(i, \sigma) \in \mathbb{N}\times\Sigma$ is given by

$$t_{\mathrm{plant},i} = \min\left\{t > t_{\mathrm{plant},i-1} : (t, s_{\sigma_{i-1}}(t, t_{\mathrm{plant},i-1}, x_{i-1})) \notin \mathcal{R}_{\sigma_{i-1}}\right\}, \tag{23}$$

where $\{\sigma_{i-1}\}_{i\in\mathbb{N}} \subset \Sigma$, $s_{\sigma_{i-1}}(\cdot, t_{\mathrm{plant},i-1}, x_{i-1})$ denotes the flow of the plant (21) and (22) originated by the $\mathcal{R}_{\sigma_{i-1}}$ resetting event at time $t_{\mathrm{plant},i-1}$ and from the initial condition x_{i-1}. In this paper, the jump map $g_{\mathrm{d},\sigma}(\cdot,\cdot)$, $\sigma \in \Sigma$, is known and uncontrollable, and the resetting events $\{\mathcal{R}_\sigma\}_{\sigma\in\Sigma} \subset \mathbb{R}^n$ are unknown. The resetting times $\{t_{\mathrm{plant},i}\}_{i\in\mathbb{N}}$ are unknown *a priori*, and are assumed to be known as soon as a resetting event in the plant occurs. With any piecewise continuous control input $u(\cdot)$, (21) and (22) are assumed to verify Assumptions 3.1 and 3.2.

Next, consider the *reference model*

$$\begin{bmatrix}\dot{x}_{\mathrm{ref}}(t)\\ \dot{\sigma}(t)\end{bmatrix} = \begin{bmatrix}A_{\mathrm{ref},\sigma(t)}x_{\mathrm{ref}}(t) + B_{\mathrm{ref},\sigma(t)}r(t)\\ 0\end{bmatrix}, \quad \begin{bmatrix}x_{\mathrm{ref}}(t_0)\\ \sigma(t_0)\end{bmatrix} = \begin{bmatrix}x_{\mathrm{ref},0}\\ \sigma_0\end{bmatrix}, \quad (t, x_{\mathrm{ref}}(t)) \notin \mathcal{R}_{\mathrm{ref},\sigma(t)}, \tag{24}$$

$$\begin{bmatrix}x_{\mathrm{ref}}(t^+)\\ \sigma(t^+)\end{bmatrix} = g_{\mathrm{d,ref},\sigma(t)}(t, x_{\mathrm{ref}}(t)), \qquad (t, x_{\mathrm{ref}}(t)) \in \mathcal{R}_{\mathrm{ref},\sigma(t)}, \tag{25}$$

where $A_{\mathrm{ref},\sigma} \in \mathbb{R}^{n\times n}$, $\sigma \in \Sigma$, is Hurwitz and such that

$$A_{\mathrm{ref},\sigma} = A_\sigma + B_\sigma K^{\mathrm{T}}_{x,\sigma} \tag{26}$$

for some $K_{x,\sigma} \in \mathbb{R}^{n\times m}$, $B_{\mathrm{ref},\sigma} \in \mathbb{R}^{n\times m}$ is such that

$$B_{\mathrm{ref},\sigma} = B_\sigma K^{\mathrm{T}}_{r,\sigma} \tag{27}$$

for some $K_{r,\sigma} \in \mathbb{R}^{m\times m}$, and the *reference command input* $r : [t_0, \infty) \to \mathbb{R}^m$ is piecewise continuous and such that $\|r(t)\| \leq r_{\max}$, where $r_{\max} \geq 0$. The reference model's dynamics, that is, $r(\cdot)$, $A_{\mathrm{ref},\sigma}$, $\sigma \in \Sigma$, and $B_{\mathrm{ref},\sigma}$ are user-defined, and their trajectories capture the desired closed-loop system's dynamics; note that since $r(\cdot)$ is piecewise continuous and bounded and $A_{\mathrm{ref},\sigma(\cdot)}$ is Hurwitz, $x_{\mathrm{ref}}(\cdot)$ is bounded between resetting events. The jump map $g_{\mathrm{d,ref},\sigma}(\cdot,\cdot)$ and the set of resetting events $\{\mathcal{R}_{\mathrm{ref},\sigma}\}_{\sigma\in\Sigma}$ are discussed in Section 5.2 below.

Finally, consider the *auxiliary model for the trajectory tracking error's transient dynamics*

$$\begin{bmatrix}\dot{e}_{\mathrm{tran}}(t)\\ \dot{\sigma}(t)\end{bmatrix} = \begin{bmatrix}A_{\mathrm{tran},\sigma(t)}e_{\mathrm{tran}}(t)\\ 0\end{bmatrix}, \qquad \begin{bmatrix}e_{\mathrm{tran}}(t_0)\\ \sigma(t_0)\end{bmatrix} = \begin{bmatrix}x_0 - x_{\mathrm{ref},0}\\ \sigma_0\end{bmatrix},$$
$$(t, e_{\mathrm{tran}}(t)) \notin \mathcal{R}_{\mathrm{tran},\sigma(t)}, \tag{28}$$

$$\begin{bmatrix}e_{\mathrm{tran}}(t^+)\\ \sigma(t^+)\end{bmatrix} = g_{\mathrm{d,tran},\sigma(t)}(t, e_{\mathrm{tran}}(t)), \qquad (t, e_{\mathrm{tran}}(t)) \in \mathcal{R}_{\mathrm{tran},\sigma(t)}, \tag{29}$$

where $A_{\mathrm{tran},\sigma} \in \mathbb{R}^{n\times n}$, $\sigma \in \Sigma$, is Hurwitz, user-defined, and such that

$$\max_{\sigma\in\Sigma}\mathrm{Re}(\lambda_{\max}(A_{\mathrm{tran},\sigma})) < \min_{\sigma\in\Sigma}\mathrm{Re}(\lambda_{\min}(A_{\mathrm{ref},\sigma})) \tag{30}$$

and

$$A_{\mathrm{tran},\sigma} = A_{\mathrm{ref},\sigma} + B_\sigma K^{\mathrm{T}}_{e,\sigma} \tag{31}$$

for some $K_{e,\sigma} \in \mathbb{R}^{n\times m}$. Condition (30) means that, in the complex plane, all the eigenvalues of the collection of matrices $\{A_{\mathrm{tran},\sigma}\}_{\sigma\in\Sigma}$ must be chosen by the user to lie to the left of the eigenvalues of any eigenvalue of any matrix in the collection $\{A_{\mathrm{ref},\sigma}\}_{\sigma\in\Sigma}$. The jump map $g_{\mathrm{d,tran},\sigma}(t, e_{\mathrm{tran}})$, $(\sigma, t, e_{\mathrm{tran}}) \in \Sigma\times[t_0, \infty)\times\mathbb{R}^n$, and the set of resetting events $\{\mathcal{R}_{\mathrm{tran},\sigma}\}_{\sigma\in\Sigma}$ are discussed in Section 5.2 below.

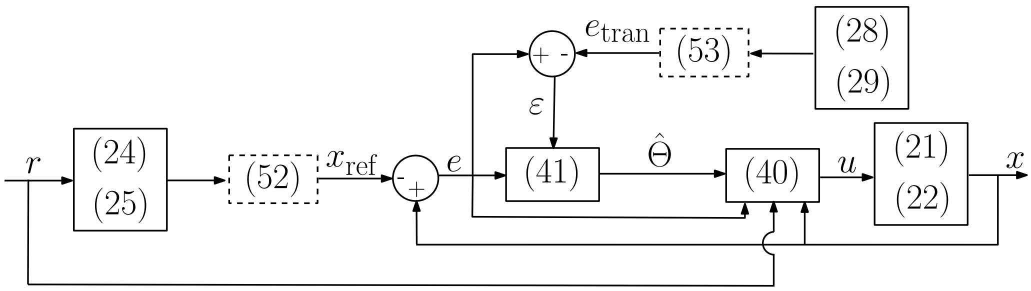

Fig. 5.1. Wire diagram of the proposed control architecture.

5.2. Control system outline

To present adaptive control laws to drive the trajectories of the plant model (21) and (22) toward the trajectories of the reference model (24) and (25), let

$$e(t) \triangleq x(t) - x_{\rm ref}(t), \qquad t \ge t_0, \tag{32}$$

$$\varepsilon(t) \triangleq e(t) - e_{\rm tran}(t), \tag{33}$$

denote the *trajectory tracking error* and the *auxiliary trajectory tracking error*, respectively. Note that if $\lim_{t\to\infty} e_{\rm tran}(t) = 0$, then $\lim_{t\to\infty} \|\varepsilon(t) - e(t)\| = 0$. The trajectory tracking error captures the relative distance of the controlled plant model from the reference model, and the auxiliary trajectory tracking error captures the difference between the closed-loop trajectory tracking error dynamics and the desired trajectory tracking error dynamics. After the transient dynamics have decayed, the auxiliary trajectory tracking error reduces to the trajectory tracking error.

Define

$$\Phi_\sigma(t,x,e) \triangleq \left[x^{\rm T}, r^{\rm T}(t), -\tilde{\Phi}_\sigma^{\rm T}(t,x), e^{\rm T}\right]^{\rm T}, \qquad (\sigma,t,x,e) \in \Sigma \times [t_0,\infty) \times \mathbb{R}^n \times \mathbb{R}^n, \tag{34}$$

$$\Theta_\sigma \triangleq \left[K_{x,\sigma}^{\rm T}, K_{r,\sigma}^{\rm T}, \tilde{\Theta}_\sigma^{\rm T}, K_{e,\sigma}^{\rm T}\right]^{\rm T}, \tag{35}$$

$$\overline{\Phi}_\sigma(t,x,e) \triangleq \left[\chi_{\Sigma_1}(\sigma)\Phi_1^{\rm T}(t,x,e), \ldots, \chi_{\Sigma_p}(\sigma)\Phi_p^{\rm T}(t,x,e)\right]^{\rm T}, \tag{36}$$

$$\Theta \triangleq \left[\Theta_1^{\rm T}, \ldots, \Theta_p^{\rm T}\right]^{\rm T}, \tag{37}$$

and $N \triangleq 2n + m + \sum_{\sigma=1}^{p} N_\sigma$, and note that

$$\begin{bmatrix}\dot{\varepsilon}(t)\\ \dot{\sigma}(t)\end{bmatrix} = \begin{bmatrix}A_{{\rm tran},\sigma(t)}\varepsilon(t) + B_{\sigma(t)}\left[u(t) - \Theta^{\rm T}\overline{\Phi}_{\sigma(t)}(t,x(t),e(t))\right]\\ 0\end{bmatrix}, \qquad \begin{bmatrix}\varepsilon(t_0)\\ \sigma(t_0)\end{bmatrix} = \begin{bmatrix}0\\ \sigma_0\end{bmatrix},$$
$$\left((t,x(t)) \notin \mathcal{R}_{\sigma(t)}\right) \wedge \left((t,x_{\rm ref}(t)) \notin \mathcal{R}_{{\rm ref},\sigma(t)}\right) \wedge \left((t,e_{\rm tran}(t)) \notin \mathcal{R}_{{\rm tran},\sigma(t)}\right), \tag{38}$$

$$\begin{bmatrix}\varepsilon(t^+)\\ \sigma(t^+)\end{bmatrix} = g_{{\rm d},\sigma(t)}(t,x(t)) - g_{{\rm d,ref},\sigma(t)}(t,x_{\rm ref}(t)) - g_{{\rm d,tran},\sigma(t)}(t,e_{\rm ref,tran}(t)),$$
$$\left((t,x(t)) \in \mathcal{R}_{\sigma(t)}\right) \vee \left((t,x_{\rm ref}(t)) \in \mathcal{R}_{{\rm ref},\sigma(t)}\right) \vee \left((t,e_{\rm tran}(t)) \in \mathcal{R}_{{\rm tran},\sigma(t)}\right), \tag{39}$$

where $\wedge$ represents the operator *and*, $\vee$ represents the operator *or*, $\Sigma_j \subseteq \Sigma$ denotes the jth out of $\sigma_{\max}$ partitions of Σ, and $\chi_{\Sigma_j} : \Sigma_j \to \{0,1\}$ symbolizes the *indicator function*.

Remark 5.1. The dynamical model (38) and (39) is employed only to prove the boundedness of $e(\cdot)$, $\varepsilon(\cdot)$, and the adaptive gains introduced later in this section, and the convergence of both $e(\cdot)$ and $\varepsilon(\cdot)$ to zero. In practice, however, $\varepsilon(\cdot)$ is deduced from (32) and (33), assuming that $x(\cdot)$ is directly measurable, $x_{\rm ref}(\cdot)$ is computed by the controller integrating (24) and (25), and $e_{\rm tran}(\cdot)$ is computed by the controller integrating (28) and (29); for details, see Fig. 5.1, which schematically captures the proposed control system.

Consider the *control law*

$$\eta(\hat{\Theta}, \overline{\Phi}_\sigma(t,x,e)) = \hat{\Theta}^{\rm T}\overline{\Phi}_\sigma(t,x,e), \qquad (\sigma,t,x,e,\hat{\Theta}) \in \Sigma \times [t_0,\infty) \times \mathbb{R}^n \times \mathbb{R}^n \times \mathbb{R}^{N\times m}, \tag{40}$$

and the *adaptive law*

$$\dot{\hat{\Theta}}(t) = -\Gamma\overline{\Phi}_{\sigma(t)}(t,x(t),e(t))\varepsilon^{\rm T}(t)P_{\sigma(t)}B_{\sigma(t)}, \qquad \hat{\Theta}(t_0) = \hat{\Theta}_0, \qquad t \ge t_0, \tag{41}$$

where the *adaptive rate matrix* $\Gamma \in \mathbb{R}^{N\times N}$ is positive-definite, $P_\sigma \in \mathbb{R}^{n\times n}$, $\sigma \in \Sigma$, is the positive-definite and such that

$$0_{n\times n} = A^{\mathrm{T}}_{\mathrm{tran},\sigma} P_\sigma + P_\sigma A_{\mathrm{tran},\sigma} + Q_\sigma, \tag{42}$$

and $Q_\sigma \in \mathbb{R}^{n\times n}$ is positive-definite. Furthermore, consider the *Lyapunov function candidate*

$$V(t,\varepsilon,\Delta\Theta) \triangleq \varepsilon^{\mathrm{T}} P_{\sigma(t)}\varepsilon + \operatorname{tr}\left(\Delta\Theta^{\mathrm{T}}\Gamma^{-1}\Delta\Theta\right), \qquad (t,\varepsilon,\Delta\Theta) \in [t_0,\infty)\times\mathbb{R}^n\times\mathbb{R}^{N\times m}, \tag{43}$$

where $\Delta\Theta(t) \triangleq \hat{\Theta}(t) - \Theta$, and define

$$W(\varepsilon) \triangleq \bar{\lambda}_{\min}\left(\{Q_\sigma\}_{\sigma\in\Sigma}\right)\|\varepsilon\|^2, \qquad \varepsilon \in \mathbb{R}^n. \tag{44}$$

The adaptive law (41) is a switched dynamical system, that is, it experiences discontinuities in its dynamics, but not in its state. Thus, the adaptive gains are computed as the Carathéodory, hence, absolutely continuous, solutions of (41). Consequently, discontinuities of $V(t,\varepsilon(t),\hat{\Theta}(t))$, $t \geq t_0$, are due to discontinuities in $P_{\sigma(t)}\varepsilon(t)$.

We define the set of resetting events of the reference model as

$$\mathcal{R}_{\mathrm{ref},\sigma_{i_w}} \triangleq \{t_{\mathrm{ref},i_w}\}\times\mathbb{R}^n, \qquad (i,w)\in\mathbb{N}\times\mathbb{N}, \tag{45}$$

where

$$t_{\mathrm{ref},i_w} \triangleq \inf\left\{ t > \max\{t_{\mathrm{plant},i}, t_{\mathrm{ref},i_w-1}\} : \int_{t_0}^{t} W(\varepsilon(\tau))\mathrm{d}\tau \geq \sum_{j=1}^{k-1}\left[V(t_j^+,\varepsilon(t_j^+),\hat{\Theta}(t_j)) - V(t_j,\varepsilon(t_j),\hat{\Theta}(t_j))\right]\right\}. \tag{46}$$

The resetting events of the auxiliary model (28) and (29) are such that

$$\mathcal{R}_{\mathrm{tran},\sigma_{i_w}} \triangleq \{t_{\mathrm{tran},i_w}\}\times\mathbb{R}^n, \qquad (i,w)\in\mathbb{N}\times\mathbb{N}, \tag{47}$$

where

$$\begin{aligned} t_{\mathrm{tran},i_{w_q}} \triangleq \inf\Bigg\{ t > \max\{t_{\mathrm{plant},i}, t_{\mathrm{ref},i_w-1}, t_{\mathrm{tran},i_{w_q}-1}\} : \int_{t_0}^{t} W(e_{\mathrm{tran}}(\tau))\mathrm{d}\tau \\ \geq \max\Bigg\{\sum_{j=1}^{k-1}\left[V(t_j^+,\varepsilon(t_j^+),\hat{\Theta}(t_j)) - V(t_j,\varepsilon(t_j),\hat{\Theta}(t_j))\right], \\ \sum_{j=1}^{k-1}\left[V_{\mathrm{tran}}(t_j^+,e_{\mathrm{tran}}(t_j^+)) - V_{\mathrm{tran}}(t_j,e_{\mathrm{tran}}(t_j))\right]\Bigg\}\Bigg\}, \end{aligned} \tag{48}$$

and

$$V_{\mathrm{tran}}(t,e_{\mathrm{tran}}) \triangleq e^{\mathrm{T}}_{\mathrm{tran}} P_{\sigma(t)} e_{\mathrm{tran}}, \qquad (t,e_{\mathrm{tran}}) \in [t_0,\infty)\times\mathbb{R}^n. \tag{49}$$

Thus, we partition the set of resetting times of (38) and (39) as $\{t_k\}_{k\in\mathbb{N}} = \{t_{\mathrm{plant},i}\}_{i\in\mathbb{N}} \cup \left(\bigcup_{i\in\mathbb{N}}\{t_{\mathrm{tran},i_w}\}_{w\in\mathbb{N}}\right) \cup \left(\bigcup_{i\in\mathbb{N}}\bigcup_{w\in\mathbb{N}}\{t_{\mathrm{ref},i_{w_q}}\}_{q\in\mathbb{N}}\right)$. Both (46) and (48) can be interpreted as conditions on the dwell times of the reference model and the auxiliary model, respectively.

Remark 5.2. To illustrate the proposed control architectures, four sets of indices are used. The index i numbers the resetting events in the plant. The index i_w numbers the resetting events in the reference model. The index i_{w_q} numbers the resetting events in the reference auxiliary model. The index k numbers all resetting events. The generic index j is reserved for summations over $\{1,\ldots,k\}$.

The jump map in (25) is defined as

$$g_{\mathrm{d,ref},\sigma}(t,x_{\mathrm{ref}}) \triangleq \left[x^{\mathrm{T}}_{\mathrm{ref}}(t^+_{\mathrm{ref},i_w}), 0\right]^{\mathrm{T}}, \qquad (\sigma,t,x_{\mathrm{ref}}) \in \Sigma\times[t_0,\infty)\times\mathbb{R}^n, \tag{50}$$

and the jump map in (29) is defined as

$$g_{\mathrm{d,tran},\sigma} \triangleq \left[e^{\mathrm{T}}_{\mathrm{tran}}(t^+_{\mathrm{tran},i_{w_q}}), 0\right]^{\mathrm{T}}, \qquad (\sigma,t,e_{\mathrm{tran}}) \in \Sigma\times[t_0,\infty)\times\mathbb{R}^n, \tag{51}$$

where

$$\begin{aligned} x_{\mathrm{ref}}(t^+_{\mathrm{ref},i_w}) &= x(t_{\mathrm{ref},i_w}) - e_{\mathrm{tran}}(t_{\mathrm{ref},i_w}) \\ &\quad - \sqrt{\frac{\varepsilon^{\mathrm{T}}(t_{\mathrm{ref},i_w})P_{\sigma(t_{\mathrm{ref},i_w})}\varepsilon(t_{\mathrm{ref},i_w}) - z_{\mathrm{ref},i_w}}{h^{\mathrm{T}}_{\mathrm{ref}}(t_{\mathrm{ref},i_w},\varepsilon(t_{\mathrm{ref},i_w}))h_{\mathrm{ref}}(t_{\mathrm{ref},i_w},\varepsilon(t_{\mathrm{ref},i_w}))}}\, P^{-\frac{1}{2}}_{\sigma(t^+_{\mathrm{ref},i_w})} h_{\mathrm{ref}}(t_{\mathrm{ref},i_w},\varepsilon(t_{\mathrm{ref},i_w})), \\ &\qquad (i,w)\in\mathbb{N}\times\mathbb{N}, \end{aligned} \tag{52}$$

$$e_{\mathrm{tran}}(t^{+}_{\mathrm{tran},i_{w_q}}) = -\sqrt{\frac{e^{\mathrm{T}}_{\mathrm{tran}}(t_{\mathrm{tran},i_{w_q}})P_{\sigma(t_{\mathrm{tran},i_{w_q}})}e_{\mathrm{tran}}(t_{\mathrm{tran},i_{w_q}}) - z_{\mathrm{tran},i_{w_q}}}{h^{\mathrm{T}}_{\mathrm{tran}}(t_{\mathrm{tran},i_{w_q}},\varepsilon(t_{\mathrm{tran},i_{w_q}}))h_{\mathrm{tran}}(t_{\mathrm{tran},i_{w_q}},\varepsilon(t_{\mathrm{tran},i_{w_q}}))}} \cdot P^{-\frac{1}{2}}_{\sigma(t^{+}_{\mathrm{tran},i_{w_q}})} h_{\mathrm{tran}}(t_{\mathrm{tran}i_{w_q}},\varepsilon(t_{\mathrm{tran},i_{w_q}})), \qquad (i,w,q)\in\mathbb{N}\times\mathbb{N}\times\mathbb{N}, \tag{53}$$

the vector functions $h_{\mathrm{ref}} : [t_0,\infty)\times\mathbb{R}^n \to \mathbb{N}^n$ and $h_{\mathrm{tran}} : [t_0,\infty)\times\mathbb{R}^n \to \mathbb{N}^n$ are such that

$$h^{\mathrm{T}}_{\mathrm{ref}}(t,\varepsilon)h_{\mathrm{ref}}(t,\varepsilon) > 0, \qquad (t,\varepsilon)\in[t_0,\infty)\times\mathbb{R}^n\setminus\{0\}, \tag{54}$$

$$h^{\mathrm{T}}_{\mathrm{tran}}(t,\varepsilon)h_{\mathrm{tran}}(t,\varepsilon) > 0, \tag{55}$$

$h_{\mathrm{ref}}(t,0)=0$, $h_{\mathrm{tran}}(t,0)=0$,

$$z_{\mathrm{ref},i_w} \in \left(0, \varepsilon^{\mathrm{T}}(t_{\mathrm{ref},i_w})P_{\sigma(t_{\mathrm{ref},i_w})}\varepsilon(t_{\mathrm{ref},i_w})\right),$$

$$z_{\mathrm{tran},i_{w_q}} \in \left(0, e^{\mathrm{T}}_{\mathrm{tran}}(t_{\mathrm{tran},i_{w_q}})P_{\sigma(t_{\mathrm{tran},i_{w_q}})}e_{\mathrm{tran}}(t_{\mathrm{tran},i_{w_q}})\right),$$

are user-defined, the series $\sum_{i=1}^{\infty}\sum_{w=1}^{\infty} z_{\mathrm{ref},i_w}$ and $\sum_{i=1}^{\infty}\sum_{w=1}^{\infty}\sum_{q=1}^{\infty} z_{\mathrm{tran},i_{w_q}}$ are convergent, and $P^{\frac{1}{2}}_{\sigma} \in \mathbb{R}^{n\times n}$, $\sigma\in\Sigma$, is symmetric, positive-definite, and such that $P_\sigma = P^{\frac{1}{2}}_{\sigma}P^{\frac{1}{2}}_{\sigma}$. The user-defined vector functions $h_{\mathrm{ref}}(\cdot,\cdot)$ and $h_{\mathrm{tran}}(\cdot,\cdot)$ can be chosen, for example, as $h_{\mathrm{ref}}(t,\varepsilon) = P^{\frac{1}{2}}_{\sigma(t)}\varepsilon$, $(t,\varepsilon)\in[t_0,\infty)\times\mathbb{R}^n$, and $h_{\mathrm{tran}}(t,\varepsilon) = P^{\frac{1}{2}}_{\sigma(t)}\varepsilon$.

Remark 5.3. The proposed control framework does not modify the mode $\sigma(\cdot)$. In the proposed approach, the mode is modified by the plant dynamics only according to (21). Indeed, it follows from (52) and (53) that $g_{\mathrm{d,ref},\sigma(t_{i_w})}(t_{i_w}, x_{\mathrm{ref}}(t_{i_w}))$ and $g_{\mathrm{d,tran},\sigma(t_{i_w})}(t_{i_w}, e_{\mathrm{tran}}(t_{i_w}))$ do not modify $\sigma(t^{+}_{i_w})$ for any $(i,w)\in\mathbb{N}\times\mathbb{N}$.

To improve the closed-loop trajectory tracking error dynamics one can set

$$e_{\mathrm{tran}}(\tilde{t}^{+}_{\mathrm{tran},i_{w_q}}) = -\varepsilon(\tilde{t}_{\mathrm{tran},i_{w_q}}), \qquad (i,w,q)\in\mathbb{N}\times\mathbb{N}\times\mathbb{N} \tag{56}$$

where $\bigcup_{i,w,q\in\mathbb{N}}\left\{\tilde{t}_{\mathrm{tran},i_{w_q}}\right\}$ denote user-defined resetting times such that $\tilde{t}_{\mathrm{tran},i_{w_q}} > \max\{t_{\mathrm{plant},i}, t_{\mathrm{ref},i_w-1}, t_{\mathrm{tran},i_{w_q}-1}\}$, $(i,w,q)\in\mathbb{N}\times\mathbb{N}\times\mathbb{N}$. This way, it follows from (33) that $x_{\mathrm{ref}}(\tilde{t}^{+}_{\mathrm{tran},i_{w_q}}) = x(\tilde{t}_{\mathrm{tran},i_{w_q}})$, that is, the trajectory tracking error $e(\cdot)$ is instantaneously set to zero, while preserving the closed-loop system's overall tracking performance. It follows from (40) and (41) that an advantage of setting the trajectory tracking error to zero by means of (56) is to instantaneously reduce the control effort and the rate of adaptation. Rearranging the indexes of the plant's resetting events, these user-defined resetting times will be considered resetting times of the plant, that is, we will set $\bigcup_{i\in\mathbb{N}}\bigcup_{w\in\mathbb{N}}\{\tilde{t}_{\mathrm{tran},i_{w_q}}\}_{q\in\mathbb{N}} \subset \bigcup_{i\in\mathbb{N}}\{t_{\mathrm{plant},i}\}_{i\in\mathbb{N}}$. Without the auxiliary model given by (28) and (29), that is, employing the hybrid control framework in [4], this result would have not been possible.

5.3. Applicability of the proposed control architecture

Fig. 5.1 and Algorithm 1 capture the proposed control architecture. In the Appendix, the two-layer MRAC system for continuous-time plants is recalled and briefly summarized by Fig. A.1 and Algorithm 3; for additional details, see [8]. Comparing Fig. 5.1 to Fig. A.1 and Algorithm 1 to Algorithm 3, it is apparent how, if the resetting set for the reference model (45) is not attained (Line 5 of Algorithm 1 is not verified) and the resetting set (47) is not attained (Line 11 of Algorithm 1 is not verified), then the proposed control system (lines 17–22 of Algorithm 1) reduces to the two-layer MRAC formulation for continuous-time systems (lines 4–9 of Algorithm 3). Therefore, the proposed hybrid architecture augments a control scheme designed for continuous-time systems by adding resetting events for the reference model (Lines 6–9 of Algorithm 1) and the auxiliary model (Lines 12–15 of Algorithm 1), while retaining the original continuous-time structure. Algorithm 2 shows an example of how to compute $\{z_{\mathrm{ref},i_w}\}_{w\in\overline{\mathbb{N}}}$, $i\in\overline{\mathbb{N}}$, and $\{z_{\mathrm{tran},i_{w_q}}\}_{q\in\overline{\mathbb{N}}}$, given some user-defined convergent series.

The fact that the proposed two-layer MRAC architecture for NHTV systems augments the two-layer MRAC architecture for continuous-time systems provides an advantage in terms of tuning the system parameters. The parameters that characterize the two-layer MRAC architecture, namely $A_{\mathrm{ref},\sigma}$, $B_{\mathrm{ref},\sigma}$, $A_{\mathrm{tran},\sigma}$, and Q_σ can be tuned for each mode $\sigma\in\Sigma$ separately employing the same approach as for continuous time-systems. The matrices $A_{\mathrm{ref},\sigma}$ and $B_{\mathrm{ref},\sigma}$ should be chosen to capture the ideal behavior of the closed-loop system in each mode $\sigma\in\Sigma$. The matrices $\{A_{\mathrm{tran},\sigma}\}_{\sigma\in\Sigma}$ should be chosen so that, in the complex plane, their eigenvalues are to the left of the eigenvalues of $\{A_{\mathrm{ref},\sigma}\}_{\sigma\in\Sigma}$. The larger is the distance between the set of eigenvalues of $\{A_{\mathrm{tran},\sigma}\}_{\sigma\in\Sigma}$ from the set of eigenvalues of $\{A_{\mathrm{ref},\sigma}\}_{\sigma\in\Sigma}$, the larger is convergence rate of the trajectory tracking error. However, as noted in [8], a larger distance between the set of eigenvalues of $\{A_{\mathrm{tran},\sigma}\}_{\sigma\in\Sigma}$ from the set of eigenvalues of $\{A_{\mathrm{ref},\sigma}\}_{\sigma\in\Sigma}$ may induce a larger overshoot in trajectory tracking error. Matrices Q_σ, $\sigma\in\Sigma$, with larger equi-induced norm facilitate the activation of the resetting conditions (45) and (47). However, larger values of $\|Q_\sigma\|$, $\sigma\in\Sigma$, usually also induce higher computational times. The adaptive rate matrix Γ can be tuned employing the same guidelines as classical MRAC [32].

In this paper, we employed geometric series for $\sum_{i=1}^{\infty}\sum_{w=1}^{\infty} z_{\mathrm{ref},i_w}$ and $\sum_{i=1}^{\infty}\sum_{w=1}^{\infty}\sum_{q=1}^{\infty} z_{\mathrm{tran},i_{w_q}}$. However, any other convergent series can be employed. Larger values of the elements of these series produce more significant reductions in the tracking error at

Algorithm 1 Algorithm for two-layer MRAC for hybrid plants

Input: $x(t)$, $\sigma(t)$ ▷ Plant state given by (21) and (22)
Output: $u(t)$ ▷ Control input with control law given by (40)
1: $k \leftarrow 0$, $i \leftarrow 0$, $i_w \leftarrow 0$, $i_{w_q} \leftarrow 0$ ▷ Initialize the reset counters
2: $x_{\mathrm{ref}}(t_0) \leftarrow x_{\mathrm{ref},0}$, $e_{\mathrm{tran}}(t_0) \leftarrow x(t_0) - x_{\mathrm{ref},0}$, $\hat{\Theta}(t_0) \leftarrow \hat{\Theta}_0$ ▷ Set the initial conditions
3: Set $B_{\mathrm{ref},\sigma_0}$, $A_{\mathrm{ref},\sigma_0}$ Hurwitz, & $A_{\mathrm{tran},\sigma_0}$ s.t. (30) is verified ▷ Initialize the reference models
4: **while** $t \geq t_0$ **do**
5: **if** $(t, x_{\mathrm{ref}}(t)) \in \mathcal{R}_{\mathrm{ref},\sigma_{i_w}}$ **then** ▷ If the resetting set (45) is reached
6: $z_{\mathrm{ref},i_w} \leftarrow$ Algorithm 2 with inputs $\varepsilon(t)$, $P_{\sigma(t)}$, z_{ref,i_w-1}
7: $i_w \leftarrow i_w + 1$, $k \leftarrow k+1$ ▷ Update the reference model counter i_w and k
8: $t_{\mathrm{ref},i_w} \leftarrow t$, $t_k \leftarrow t$ ▷ Update resetting times
9: $x_{\mathrm{ref}}(t_k) \leftarrow$ right-hand side of (53) ▷ Induce variation in the reference trajectory
10: **end if**
11: **if** $(t, e_{\mathrm{tran}}(t)) \in \mathcal{R}_{\mathrm{tran},\sigma_{i_{w_q}}}$ **then** ▷ If the resetting set (47) is reached
12: $z_{\mathrm{tran},i_{w_q}} \leftarrow$ Algorithm 2 with inputs $e_{\mathrm{tran}}(t)$, $P_{\sigma(t)}$, k
13: $i_{w_q} \leftarrow i_{w_q} + 1$, $k \leftarrow k+1$ ▷ Update the second layer counter i_{w_q} and k
14: $t_{\mathrm{tran},i_{w_q}} \leftarrow t$, $t_k \leftarrow t$ ▷ Update resetting times
15: $e_{\mathrm{tran}}(t_k) \leftarrow$ right-hand side of (53) ▷ Induce variation in the second layer
16: **end if**
17: $x_{\mathrm{ref}}(t) \leftarrow \int_{t_k}^{t} \left(A_{\mathrm{ref},\sigma(t)} x_{\mathrm{ref}}(t) + B_{\mathrm{ref},\sigma(t)} r(t)\right) \mathrm{d}\tau + x_{\mathrm{ref}}(t_k)$ ▷ Apply (24)
18: $e_{\mathrm{tran}}(t) \leftarrow \int_{t_k}^{t} A_{\mathrm{tran},\sigma(\tau)} e_{\mathrm{tran}}(\tau)\mathrm{d}\tau + x(t_k) - x_{\mathrm{ref}}(t_k)$ ▷ Apply (28)
19: $e(t) \leftarrow x(t) - x_{\mathrm{ref}}(t)$ ▷ Compute the trajectory tracking error
20: $\varepsilon(t) \leftarrow e(t) - e_{\mathrm{tran}}(t)$ ▷ Compute the error from the second layer
21: $\hat{\Theta}(t) \leftarrow -\int_{t_0}^{t} \Gamma \overline{\Phi}_{\sigma(\tau)}(t, x(\tau), e(\tau)) \varepsilon^{\mathrm{T}}(\tau) P_{\sigma(\tau)} B_{\sigma(\tau)} \mathrm{d}\tau + \hat{\Theta}_0$ ▷ Apply (41)
22: $u(t) \leftarrow \eta(\hat{\Theta}(t), \overline{\Phi}_{\sigma(t)}(t, x(t), e(t)))$ ▷ Apply (40)
23: **end while**

Algorithm 2 Algorithm to find z_{ref,i_w} and $z_{\mathrm{tran},i_{w_q}}$ (See lines 6 and 12 in Algorithm 1)

Input: e, P, k_{previous}
Output: z
This algorithm assumes, *for example*, that the underlying series has generic element $z = k^{-\alpha}$ with $\alpha > 1$ and $k \in \mathbb{N}$. Alternative convergent series can be used
1: $k = \max\left\{\left\lceil \left(e^{\mathrm{T}} P e\right)^{-\frac{1}{\alpha}} \right\rceil, k_{\mathrm{previous}} + 1\right\}$
2: $z = k^{-\alpha}$

the resetting events (45) and (47). The faster $\left\{z_{\mathrm{ref},i_w}\right\}_{i_w}$ and $\left\{z_{\mathrm{tran},i_{w_q}}\right\}_{i_{w_q}}$ converge to zero, the sooner the effect of the proposed resetting mechanisms decays. To overcome this problem, these series can be reset. However, series must not be reset infinitely many times in any finite-time interval.

5.4. Effectiveness of the proposed control architecture

In this section, we present the main result of this paper. It follows from (21), (22), (24) and (25) that the trajectory tracking error dynamics are given by

$$\begin{bmatrix}\dot{e}(t)\\ \dot{\sigma}(t)\end{bmatrix} = \begin{bmatrix} A_{\mathrm{ref},\sigma(t)} e(t) + B_{\sigma(t)}\left[u(t) - \Theta^{\mathrm{T}} \overline{\Phi}_{\sigma(t)}(t, x(t), e(t))\right] \\ 0 \end{bmatrix}, \quad \begin{bmatrix} e(t_0) \\ \sigma(t_0)\end{bmatrix} = \begin{bmatrix} x_0 - x_{\mathrm{ref},0} \\ \sigma_0 \end{bmatrix},$$
$$\left((t, x(t)) \notin \mathcal{R}_{\sigma(t)}\right) \wedge \left((t, x_{\mathrm{ref}}(t)) \notin \mathcal{R}_{\mathrm{ref},\sigma(t)}\right), \tag{57}$$

$$\begin{bmatrix} e(t^+) \\ \sigma(t^+) \end{bmatrix} = g_{\mathrm{d},\sigma(t)}(t, x(t)) - g_{\mathrm{d,ref},\sigma(t)}(t, x_{\mathrm{ref}}(t)),$$
$$\left((t, x(t)) \in \mathcal{R}_{\sigma(t)}\right) \vee \left((t, x_{\mathrm{ref}}(t)) \in \mathcal{R}_{\mathrm{ref},\sigma(t)}\right). \tag{58}$$

The next result shows that if $u(t) = \eta(\hat{\Theta}(t), \overline{\Phi}_\sigma(t, x(t)))$, $t \geq t_0$, $\hat{\Theta}(\cdot)$ verifies (41), the reference trajectory $x_{\mathrm{ref}}(\cdot)$ is reset according to (52) whenever the resetting condition (45) is met, and the auxiliary variable $e_{\mathrm{tran}}(\cdot)$ is reset according to (53) whenever the resetting condition (47) is met, then $e(\cdot)$ and $\hat{\Theta}(\cdot)$ are uniformly bounded, and the rate of convergence of the trajectory tracking error is such that

$$\alpha_{\max}(e(\cdot)) \geq \alpha, \tag{59}$$

where $\alpha > -\mathrm{Re}(\lambda_{\min}(A_{\mathrm{ref}})) \geq -\mathrm{Re}(\lambda_{\max}(A_{\mathrm{ref}}))$ is a user-defined parameter.

Theorem 5.1. *Consider the plant model (21) and (22) with $u(t) = \eta(\hat{\Theta}(t), \overline{\Phi}_\sigma(t, x(t)))$, $t \geq t_0$, and adaptive law (41), the reference model (24) and (25) with set of resetting events given by (45), and the auxiliary model (28) and (29) with set of resetting events given by (47). Let $\mathrm{Re}(\lambda_{\max}(A_{\mathrm{tran},\sigma})) < \mathrm{Re}(\lambda_{\min}(A_{\mathrm{ref},\sigma}))$, $\sigma \in \Sigma$. Then, both the trajectory tracking error $e(\cdot)$ and the adaptive gain matrix $\hat{\Theta}(\cdot)$ are bounded uniformly in $\{t_k\}_{k\in\overline{\mathbb{N}}}$, and $e(t) \to 0$ as $t \to \infty$ for all $e_0 \in \mathbb{R}^n$ uniformly in $\{t_k\}_{k\in\overline{\mathbb{N}}}$. Furthermore, (59) is verified with $\alpha > -\min_{\sigma\in\Sigma} \mathrm{Re}(\lambda_{\min}(A_{\mathrm{ref},\sigma}))$.*

Proof. Consider the Lyapunov function candidate (43). By applying Theorem 3.2 and proceeding as in the proof of Theorem 4 of [4], it is possible to prove that every maximal solution $\varepsilon(\cdot)$ of (38) and (39) is uniformly bounded in $\{t_k\}_{k\in\overline{\mathbb{N}}}$, $\hat{\Theta}(\cdot)$ is uniformly bounded in $\{t_k\}_{k\in\overline{\mathbb{N}}}$, and $\varepsilon(t) \to 0$ as $t \to \infty$ uniformly in $\{t_k\}_{k\in\overline{\mathbb{N}}}$. This passage is omitted for brevity.

Next, note that

$$\bar{\lambda}_{\min}\left(\{P_\sigma\}_{\sigma\in\Sigma}\right) \|e_{\mathrm{tran}}\|^2 \leq V_{\mathrm{tran}}(t, e_{\mathrm{tran}}) \leq \bar{\lambda}_{\max}\left(\{P_\sigma\}_{\sigma\in\Sigma}\right) \|e_{\mathrm{tran}}\|^2, \quad (t, e_{\mathrm{tran}}) \in [t_0, \infty) \times \mathbb{R}^n, \tag{60}$$

and

$$\dot{V}_{\mathrm{tran}}(t, e_{\mathrm{tran}}(t)) = -W(e_{\mathrm{tran}}(t)), \qquad t \in [t_0, \infty). \tag{61}$$

Furthermore, note that the condition (11) on the critical times of (28) and (29) is always verified, since discontinuities occur at the critical times only. By proceeding as in the Proposition 3 of [4], we verify that

$$\sum_{k=1}^{\infty}\left[V_{\mathrm{tran}}(t_k^+, e_{\mathrm{tran}}(t_k^+)) - V_{\mathrm{tran}}(t_k, e_{\mathrm{tran}}(t_k))\right] = -\sum_{i=1}^{\infty}\sum_{w=1}^{\infty}\sum_{q=1}^{\infty} z_{\mathrm{tran},i_{w_q}}. \tag{62}$$

Therefore, it follows from Theorem 3.2 that $e_{\mathrm{tran}}(\cdot)$ is bounded and $e_{\mathrm{tran}}(t) \to 0$ as $t \to \infty$ uniformly in $t_0 \in [0, \infty)$ and $\{t_k\}_{k\in\mathbb{N}}$.

By the triangle inequality [5, Def. 2.6], it holds that

$$\|\varepsilon(t)\| \geq \left| \|e(t)\| - \|e_{\mathrm{tran}}(t)\| \right|, \qquad t \geq t_0. \tag{63}$$

Since both $\varepsilon(\cdot)$ and $e_{\mathrm{tran}}(\cdot)$ are uniformly bounded, and $\varepsilon(t) \to 0$ and $e_{\mathrm{tran}}(t) \to 0$ as $t \to \infty$ uniformly in $t_0 \in [0, \infty)$ and $\{t_k\}_{k\in\mathbb{N}}$, $e(\cdot)$ is uniformly bounded and $e(t) \to 0$ as $t \to \infty$ uniformly in $t_0 \in [0, \infty)$ and $\{t_k\}_{k\in\mathbb{N}}$.

Finally, $\Delta\Theta^{\mathrm{T}}(t)\overline{\Phi}_{\sigma(t)}(t, x(t), e(t))$, $t \geq t_0$, $t \geq t_0$, is a bounded control input for (38) and (39) with $u(t) = \eta(\hat{\Theta}(t), \overline{\Phi}_\sigma(t, x(t)))$. Since $e(t) = \varepsilon(t) + e_{\mathrm{tran}}(t)$, $t \geq t_0$, and $\log(\alpha + \beta) = \log\alpha + \log\left(1 + \beta\alpha^{-1}\right)$ for all $\alpha, \beta > 0$, it follows from (28) and (29), (38) and (39), and Lemma 4.1 that there exist $\xi : [t_0, \infty) \to \mathbb{R}$, $\gamma_1 \geq 1$, and $\gamma_2 \in (0, 1)$ such that $\lim_{t\to\infty} \xi(t) = \max_{\sigma\in\Sigma} \mathrm{Re}(\lambda_{\max}(A_{\mathrm{tran},\sigma}))$ and

$$\log(\|e(t)\|) \leq \log\left(\gamma_1\|x_0 - x_{\mathrm{ref},0}\|\right) + \xi(t)(t - t_0) + \log\Bigg(1 - \frac{\gamma_1\|B_{\sigma(t)}\|}{\gamma_2 \max_{\sigma\in\Sigma}\mathrm{Re}(\lambda_{\max}(A_{\mathrm{tran},\sigma}))} \cdot \sup_{\tau\in[t_0,\infty)} \left\|\Delta\Theta^{\mathrm{T}}(\tau)\overline{\Phi}_{\sigma(\tau)}(\tau, x(\tau), e(\tau))\right\| \left[e^{\xi(t)(t-t_0)}\gamma_1\|x_0 - x_{\mathrm{ref},0}\|\right]^{-1}\Bigg), \quad t \in [t_0, \infty) \setminus \bigcup_{k\in\mathbb{N}}\{t_k\}. \tag{64}$$

Now, since $\lim_{t\to\infty} \dfrac{\log\left(1 - \zeta e^{\lambda(t-t_0)}\right)}{t_0 - t} = 0$ for all $\zeta > 0$ and $\lambda < 0$, $\lim_{t\to\infty} e(t) = 0$ uniformly in $\{t_k\}_{k\in\overline{\mathbb{N}}}$, and, by Lemma 4.1, it holds that $\liminf_{t\to\infty} \xi(t) \geq \max_{\sigma\in\Sigma} \mathrm{Re}(\lambda_{\max}(A_{\mathrm{tran},\sigma}))$, it follows from Definition 4.1, (64), and (30) that

$$\begin{aligned}\alpha_{\max}(e(\cdot)) &\geq -\max_{\sigma\in\Sigma} \mathrm{Re}(\lambda_{\max}(A_{\mathrm{tran},\sigma})) \\ &> -\mathrm{Re}(\lambda_{\min}(A_{\mathrm{ref},\sigma})) \\ &\geq -\mathrm{Re}(\lambda_{\max}(A_{\mathrm{ref},\sigma})) > 0, \ \sigma \in \Sigma,\end{aligned} \tag{65}$$

and the result is proven. ■

Theorem 5.1 captures the key original contribution of this paper, namely an MRAC system for NTVH plants affected by parametric and matched uncertainties. In particular, consider the NTVH system with continuous-time dynamics given by (21) with $u(t) = \eta(\hat{\Theta}(t), \overline{\Phi}_\sigma(t, x(t)))$, $t \geq t_0$, (41), (24), and (28), and with discrete-time dynamics given by (22), (25), and (29). Theorem 5.1 proves uniform boundedness of the trajectory tracking error $e(\cdot)$ and of the adaptive gains $\hat{\Theta}(\cdot)$, and convergence of the trajectory tracking error $e(\cdot)$ to zero uniformly in the series of resetting times $\{t_k\}_{k\in\overline{N}}$. Furthermore, Theorem 5.1 proves that a user-defined rate of convergence of $e(\cdot)$ can be imposed by choosing the eigenvalues of $\left\{A_{\mathrm{tran},\sigma}\right\}_{\sigma\in\Sigma}$. The implementation of this system is illustrated by Fig. 5.1 and Algorithm 1. The next two results prove uniform boundedness of the auxiliary error and of the reference trajectory.

Theorem 5.2. *Consider the reference model (28) and (29) with set of resetting events given by (47). The reference trajectory $e_{\rm tran}(\cdot)$ is bounded uniformly in $\{t_k\}_{k\in\overline{\mathbb{N}}}$ and $\lim_{t\to\infty} e_{\rm tran}(t)=0$ uniformly in $\{t_k\}_{k\in\overline{\mathbb{N}}}$.*

Proof. Consider the Lyapunov-like function $V_{\rm tran}(\cdot,\cdot)$ given by (49). This function is continuously differentiable and radially unbounded, and, hence, (9) is verified with $W_1(e_{\rm tran}) = V_{\rm tran}(t,e_{\rm tran}) = W_2(e_{\rm tran})$, $(t,e_{\rm tran})\in[t_0,\infty)\times\mathcal{Z}$, and $\mathcal{Z}=\mathbb{R}^n$. Next, along the trajectories of (28) and (29), it holds that

$$\dot V_{\rm tran}(t,e_{\rm tran}) = -e_{\rm tran}^{\rm T} Q_{\sigma(t)} e_{\rm tran} \le -\bar\lambda_{\min}\left(\{Q_\sigma\}_{\sigma\in\Sigma}\right)\|e_{\rm tran}\|^2<0, \qquad (t,e_{\rm ref})\notin\bigcup_{\sigma\in\Sigma}\mathcal{R}_{{\rm tran},\sigma}, \tag{66}$$

where $\mathcal{R}_{{\rm tran},\sigma}$ is given by (47), Hence, (12) is verified with $W(x)=\bar\lambda_{\min}\left(\{Q_\sigma\}_{\sigma\in\Sigma}\right)\|e_{\rm tran}\|^2$. Furthermore, Assumptions 3.1 and 3.2 are verified, since, by (48), $t_{{\rm tran},i_{w_q}} > t_{{\rm tran},i_{w_q}-1}$ for all $(i,w,q)\in\mathbb{N}\times\mathbb{N}\times\mathbb{N}$. Finally, since (62) is verified, the result follows from Theorem 3.2. ■

Theorem 5.3. *Consider the reference model (24) and (25) with set of resetting events given by (45). The reference trajectory $x_{\rm ref}(\cdot)$ is bounded uniformly in $\{t_k\}_{k\in\overline{\mathbb{N}}}$.*

Proof. Consider the Lyapunov-like function

$$V_{\rm ref}(t,x_{\rm ref}) \triangleq x_{\rm ref}^{\rm T} P_{\sigma(t)} x_{\rm ref}, \qquad (t,x_{\rm ref})\in[t_0,\infty)\times\mathbb{R}^n, \tag{67}$$

where $P_\sigma\in\mathbb{R}^{n\times n}$ is the symmetric, positive-definite solution of

$$A_{{\rm ref},\sigma}^{\rm T} P_\sigma + P_\sigma A_{{\rm ref},\sigma} = -Q_\sigma, \qquad \sigma\in\Sigma. \tag{68}$$

The function $V_{\rm ref}(\cdot,\cdot)$ is continuously differentiable and radially unbounded, and (9) is verified with $\mathcal{Z}=\mathbb{R}^n$, $W_1(x_{\rm ref}) = \bar\lambda_{\min}\left(\{P_\sigma\}_{\sigma\in\Sigma}\right)$, and $W_2(x_{\rm ref})=\bar\lambda_{\max}\left(\{P_\sigma\}_{\sigma\in\Sigma}\right)$ for all $(t,x_{\rm ref})\in[t_0,\infty)\times\mathcal{Z}$.

Along the trajectories of (24) and (25), it holds that

$$\begin{aligned}\dot V(t,x_{\rm ref}) &\le -x_{\rm ref}^{\rm T} Q_{\sigma(t)} x_{\rm ref} + 2\|B_{{\rm ref},\sigma}\|\|P_{\sigma(t)}\|\|x_{\rm ref}\|\|r(t)\| \\ &\le -\bar\lambda_{\min}\left(\{Q_\sigma\}_{\sigma\in\Sigma}\right)\|x_{\rm ref}\|^2 + 2r_{\max}\max_{\sigma\in\Sigma}\left(\|B_{{\rm ref},\sigma}\|\|P_\sigma\|\right)\|x_{\rm ref}\| \\ &<0, \qquad (t,x_{\rm ref})\notin\left([t_0,\infty)\times\left(\mathcal{Z}\setminus\overline{\mathcal{A}}_{\rm ref}\right)\right)\cap\left(\bigcup_{\sigma\in\Sigma}\mathcal{R}_{{\rm ref},\sigma}\right),\end{aligned} \tag{69}$$

where $\mathcal{R}_{{\rm ref},\sigma}$ is given by (45) and

$$\overline{\mathcal{A}}_{\rm ref} \triangleq \left\{x_{\rm ref}\in\mathbb{R}^n : \|x_{\rm ref}\| \le 2r_{\max}\frac{\max_{\sigma\in\Sigma}\left(\|B_{{\rm ref},\sigma}\|\|P_\sigma\|\right)}{\bar\lambda_{\min}\left(\{Q_\sigma\}_{\sigma\in\Sigma}\right)}\right\} \tag{70}$$

is compact. Furthermore, Assumptions 3.1 and 3.2 are verified, since, by (46), $t_{{\rm ref},i_w} > t_{{\rm ref},i_w-1}$ for all $(i,w)\in\mathbb{N}\times\mathbb{N}$.

To prove that $\sum_{k=1}^\infty \left[V_{\rm ref}(t_k^+,x_{\rm ref}(t_k^+)) - V(t_k,x_{\rm ref}(t_k))\right]$, we note that

$$\sum_{k=1}^\infty \left[V_{\rm ref}(t_k^+,x_{\rm ref}(t_k^+)) - V(t_k,x_{\rm ref}(t_k))\right] = \lim_{k\to\infty} x_{\rm ref}^{\rm T}(t_k^+)P_{\sigma(t_k^+)}x_{\rm ref}(t_k^+) - x_{\rm ref}^{\rm T}(t_1)P_{\sigma(t_1)}x_{\rm ref}(t_1). \tag{71}$$

Now, $\lim_{k\to\infty} z_{{\rm ref},k}=0$ since $\sum_{i=1}^\infty\sum_{w=1}^\infty z_{{\rm ref},i_w} = \sum_{k=1}^\infty z_{{\rm ref},k}$ is finite, and $\lim_{k\to\infty} e_{\rm tran}(t_k)=0$ by Theorem 5.2. Therefore, it follows from (52) that $\lim_{k\to\infty}\|x_{\rm ref}(t_k^+)-x(t_k)\|=0$. It follows from Theorem 5.1 that $\lim_{t\to\infty}\|x_{\rm ref}(t)-x(t)\|=0$ uniformly in $\{t_k\}_{k=1}^\infty$, which implies that $\lim_{k\to\infty}\|x_{\rm ref}(t_k^+)-x_{\rm ref}(t_k)\|=0$. Consequently,

$$\begin{aligned}\sum_{k=1}^\infty \left[V_{\rm ref}(t_k^+,x_{\rm ref}(t_k^+)) - V(t_k,x_{\rm ref}(t_k))\right] &= \lim_{k\to\infty} x_{\rm ref}^{\rm T}(t_k)P_{\sigma(t_k^+)}x_{\rm ref}(t_k) - x_{\rm ref}^{\rm T}(t_1)P_{\sigma(t_1)}x_{\rm ref}(t_1) \\ &\le \bar\lambda_{\max}\left(\{P_\sigma\}_{\sigma\in\Sigma}\right)\lim_{k\to\infty}\|x_{\rm ref}(t_k)\|^2.\end{aligned} \tag{72}$$

As discussed in Remark 5.3, the mode $\sigma(\cdot)$ changes only if the plant model changes. Hence, $A_{{\rm ref},\sigma}$, $B_{{\rm ref},\sigma}$, Q_σ, and P_σ may vary only upon a resetting event of the plant model, and the convergence properties of the sequence $\{x_{\rm ref}(t_k)\}_{k=1}^\infty$ are the same as the convergence properties as the subsequence $\{x_{\rm ref}(t_{i_w})\}_{w=1}^\infty$. Thus, $\lim_{k\to\infty}\|x_{\rm ref}(t_k)\| = \lim_{w\to\infty}\|x_{\rm ref}(t_{i_w})\|<\infty$ since $r(\cdot)$ is bounded by assumption and $A_{{\rm ref},\sigma_{i_w}}$ is Hutwitz. The result now follows from Theorem 3.1. ■

The proof of Theorem 5.1–Theorem 5.3 reveal that the proposed control system is effective for any initial condition in the plant state, the reference mode, the auxiliary model, and the adaptive gain matrices. Indeed, Theorem 5.1–Theorem 5.3 apply to dynamical systems, whose domain is defined on the entire state space and the underlying Lyapunov-like functions are positive-definite, radially unbounded, and decrescent.

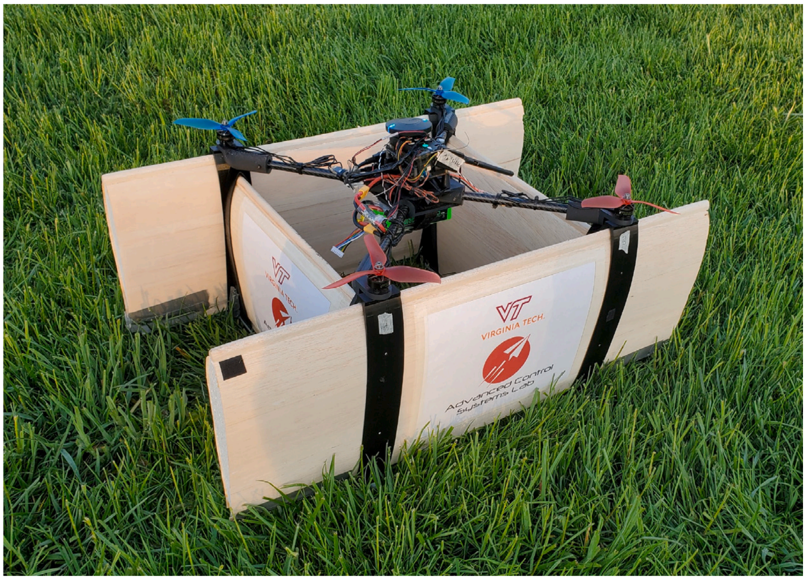

Fig. 6.1. Prototype of a tailsitter UAV, whose controller is discussed in this paper. The vehicle is equipped with four push propellers, and two NACA0012 wings.

6. Numerical examples

In this section, numerical simulations show both the applicability of the proposed two-layer MRAC system for NTVH dynamical systems and its advantages over classical MRAC [7, Ch. 9] and the hybrid MRAC system presented in [4] and summarized in Appendix.

6.1. Longitudinal dynamics of a quad-biplane

Quad-biplane UAVs are multi-rotor aircraft equipped with four collinear propellers and two parallel wings; see Fig. 6.1 for a prototype. An advantage of these vehicles lies in their ability to take off and land vertically and hover like quadcopters and exploit their wings to generate lift and cover long distances like fixed-wing aircraft. A challenge in the control of quad-biplanes lies in the fact that these vehicles' dynamics change substantially, depending on whether the wings operate in a linear regime, and, hence, produce appreciable lift, or operate in nonlinear regime and are affected by substantial drag. The difference between the linear and the nonlinear regime for the wings is so significant and occurs so rapidly across the stall angle that this vehicle's dynamics are best captured by a hybrid model. In this section, we propose a hybrid controller for the outer loop longitudinal dynamics of a quadbiplane.

Problem Statement

Consider the inertial, right-handed, orthonormal reference frame $\mathbb{I} \triangleq \{O; X, Y, Z\}$ centered at $O \triangleq 0_3$ with Z pointing down, that is, such that the weight of the UAV is given by mgZ, where $m > 0$ denotes the mass of the UAV and $g > 0$ denotes the gravitational acceleration. Let $\mathbb{J}(\cdot) \triangleq \{p(\cdot); x(\cdot), y(\cdot), z(\cdot)\}$ denote an orthonormal right-handed reference frame fixed with the UAV, where $p(t) \triangleq \left[p_X(t), p_Y(t), p_Z(t)\right]^{\mathrm{T}}$ denotes the position of the center of mass of the UAV relative to O, and $x, y, z : [t_0, \infty) \to \mathbb{R}^3$ denote the roll, pitch, and yaw axes of the UAV, respectively. Let $\theta : [t_0, \infty) \to \mathbb{R}$ denote the UAV's *pitch angle*, that is, the angle between X and $x(\cdot)$, assuming that the roll and yaw angles are equal to zero at all times. Let $q(t) \triangleq \dot{\theta}(t)$ denote the *pitch rate*, let $V_X : [t_0, \infty) \to \mathbb{R}$ denote the *translational velocity* along X, let $V_Z : [t_0, \infty) \to \mathbb{R}$ denote the *translational velocity* along Z, let $\|V(t)\| \triangleq \sqrt{V_X^2(t) + V_Z^2(t)}$, $t \geq t_0$, and let

$$\alpha(t) \triangleq \mathrm{atan2}\left(V_X(t)\sin\theta(t) + V_Z(t)\cos\theta(t), V_X(t)\cos\theta(t) - V_Z(t)\sin\theta(t)\right) \tag{73}$$

denote the *angle of attack* of the UAV, where $\mathrm{atan2} : (\mathbb{R} \times \mathbb{R}) \setminus \{(0,0)\} \to \mathbb{R}$ denotes the signed arc-tangent function. In the following, we assume that the UAV is controlled only by means of the *total thrust* $T : [t_0, \infty) \to \mathbb{R}$, which operates along $x(\cdot)$, and the *moment of the thrust* $M : [t_0, \infty) \to \mathbb{R}$.

If the wings of the UAV use a symmetric airfoil and $\alpha(t) \in \left(-\alpha_{\mathrm{stall}}, \alpha_{\mathrm{stall}}\right)$, where $\alpha_{\mathrm{stall}} > 0$ denotes the stall angle of the wing, then the UAV is said to operate in *biplane mode*. In this mode, the linearized longitudinal dynamics of the UAV are captured by

$$\begin{bmatrix} \dot{\theta}(t) \\ \dot{V}_X(t) \\ \dot{V}_Z(t) \\ \dot{q}(t) \end{bmatrix} = A_1 \begin{bmatrix} \theta(t) \\ V_X(t) \\ V_Z(t) \\ q(t) \end{bmatrix} + B_1 \begin{bmatrix} T(t) \\ M(t) \end{bmatrix}, \qquad \begin{bmatrix} \theta(t_0) \\ V_X(t_0) \\ V_Z(t_0) \\ q(t_0) \end{bmatrix} = \begin{bmatrix} \theta_0 \\ V_{X,0} \\ V_{Z,0} \\ q_0 \end{bmatrix}, \qquad t \geq t_0, \tag{74}$$

where

$$A_1 \triangleq \begin{bmatrix} 0 & 0 & 0 & 1 \\ -g\cos\theta_{\mathrm{e},1} & a_{2,2,1} & a_{2,3,1} & 0 \\ -g\sin\theta_{\mathrm{e},1} & a_{3,2,1} & a_{3,3,1} & a_{3,4,1} \\ a_{4,1,1} & a_{4,2,1} & a_{4,3,1} & a_{4,4,1} \end{bmatrix}, \quad B_1 \triangleq \begin{bmatrix} 0 & 0 \\ m^{-1}\cos\theta_{\mathrm{e},1} & 0 \\ -m^{-1}\sin\theta_{\mathrm{e},1} & 0 \\ 0 & I_y^{-1} \end{bmatrix},$$

$a_{2,2,1}, a_{2,3,1}, a_{3,2,1}, a_{3,3,1}, a_{3,4,1}, a_{4,1,1}, a_{4,2,1}, a_{4,3,1}, a_{4,4,1} \in \mathbb{R}$ denote aerodynamic coefficients, which are unknown, $\theta_{\mathrm{e},1} \in \mathbb{R}$ denotes the pitch angle at equilibrium in biplane mode, and $I_y > 0$ denotes the moment of inertia about the pitch axis [33, Ch. 2].

If $|\alpha(t)| > \alpha_{\mathrm{stall}}$, then the UAV is said to operate in *quadcopter mode*. In this mode, the longitudinal dynamics of the UAV are captured by

$$\begin{bmatrix} \dot\theta(t) \\ \dot V_X(t) \\ \dot V_Z(t) \\ \dot q(t) \end{bmatrix} = A_2 \begin{bmatrix} \theta(t) \\ V_X(t) \\ V_Z(t) \\ q(t) \end{bmatrix} + B_2\left(\begin{bmatrix} T(t) \\ M(t) \end{bmatrix} - \rho S \begin{bmatrix} 0.5C_{\mathrm{D},0} & k \\ 0.5C_{\mathrm{D},0}\bar c & k\bar c \end{bmatrix} \begin{bmatrix} 1 \\ \sin^4(\alpha(t))\cos^2(\alpha(t)) \end{bmatrix} \|V(t)\|^2 \right),$$

$$\left[\theta(t_0), V_X(t_0), V_Z(t_0), q(t_0)\right]^{\mathrm{T}} = \left[\theta_0, V_{X,0}, V_{Z,0}, q_0\right]^{\mathrm{T}}, \qquad t \ge t_0, \tag{75}$$

where

$$A_2 \triangleq \begin{bmatrix} 0 & 0 & 0 & 1 \\ -g\cos\theta_{\mathrm{e},2} & 0 & 0 & 0 \\ -g\sin\theta_{\mathrm{e},2} & 0 & 0 & 0 \\ 0 & 0 & 0 & 0 \end{bmatrix}, \quad B_2 \triangleq \begin{bmatrix} 0 & 0 \\ m^{-1}\cos\theta_{\mathrm{e},2} & 0 \\ -m^{-1}\sin\theta_{\mathrm{e},2} & 0 \\ 0 & I_y^{-1} \end{bmatrix},$$

$\theta_{\mathrm{e},2} \in \mathbb{R}$ denotes the pitch angle at equilibrium in quadcopter mode, $\rho > 0$ denotes the *air density*, $S > 0$ denotes the *reference surface area*, $C_{\mathrm{D},0} > 0$ denotes the *drag coefficient at zero angle of attack*, $\bar c > 0$ denotes the distance of the aerodynamic center from the UAV's center of mass, $k \triangleq (\pi \mathrm{AR})^{-1}$, and $\mathrm{AR} > 0$ denotes the wing's *aspect ratio*; in this paper, we consider ρ, S, $C_{\mathrm{D},0}$, $\bar c$, and k unknown. The case of an asymmetric airfoil can be readily deduced from the model considered herein. The model of the aerodynamic force in quadcopter mode has been deduced from [34].

Since the dynamical models (74) and (75) are under-actuated, their control architecture must be separated into an outer loop and an inner loop [35]. The outer-loop dynamics are given by

$$\begin{bmatrix} \dot V_X(t) \\ \dot V_Z(t) \end{bmatrix} = \begin{bmatrix} a_{2,2,\sigma(t)} & a_{2,3,\sigma(t)} \\ a_{3,2,\sigma(t)} & a_{3,3,\sigma(t)} \end{bmatrix} \begin{bmatrix} V_X(t) \\ V_Z(t) \end{bmatrix} + m^{-1}\left(\begin{bmatrix} \tilde T_x(t) \\ \tilde T_z(t) \end{bmatrix} + m \begin{bmatrix} -g\cos\theta_{\mathrm{e},\sigma(t)} & 0 \\ -g\sin\theta_{\mathrm{e},\sigma(t)} & a_{3,4,\sigma(t)} \end{bmatrix} \begin{bmatrix} \theta(t) \\ \dot\theta(t) \end{bmatrix} + \tilde\Theta^{\mathrm{T}}_{\sigma(t)} \tilde\Phi_{\sigma(t)}(t, x(t)) \right),$$

$$\begin{bmatrix} V_X(t_0) \\ V_Z(t_0) \end{bmatrix} = \begin{bmatrix} V_{X,0} \\ V_{Z,0} \end{bmatrix}, \qquad t \ge t_0, \tag{76}$$

where $x(t) = \left[V_X(t), V_Z(t)\right]^{\mathrm{T}}$, $\left[\tilde T_x, \tilde T_z\right]^{\mathrm{T}} : [t_0, \infty) \to \mathbb{R}^2$ denotes the thrust force that should be applied in the case the thrust force could be oriented at will,

$$T(t) \triangleq \left\| \left[\tilde T_x(t), \tilde T_z(t)\right]^{\mathrm{T}} \right\|,$$

$a_{i,j,\sigma}$ denotes the element on the ith row and jth column of A_σ, $\tilde\Phi_1(t,x) = 0_2$, $(t,x) \in [t_0,\infty) \times \mathbb{R}^4$, $\tilde\Phi_2(t,x) = -\begin{bmatrix} 1 \\ \sin^4(\alpha(t))\cos^2(\alpha(t)) \end{bmatrix}$ $\|V(t)\|^2$, $\tilde\Theta_1 = 0_{2\times 2}$, and $\tilde\Theta_2 = \rho S \begin{bmatrix} 0.5C_{\mathrm{D},0} & k \\ 0.5C_{\mathrm{D},0}\bar c & k\bar c \end{bmatrix}^{\mathrm{T}}$. The inner loop regulates the UAV's pitch angle so that $\lim_{t\to\infty} |\theta(t) - \theta_{\mathrm{user}}(t)| = 0$, where

$$\theta_{\mathrm{user}}(t) \triangleq \operatorname{atan2}\left(\tilde T_z(t), \tilde T_x(t)\right), \qquad t \ge t_0.$$

The problems of regulating the inner loop dynamics and integrating inner and outer loops are omitted for conciseness and to better highlight the applicability of the proposed theoretical framework. Thus, in the following, we assume for simplicity that $\theta(t) \equiv \theta_{\mathrm{user}}(t)$, $t \ge t_0$.

The dynamical model (76) is in the same form as (21) with $n = 2$, $m = 2$, $N = 4$, $\mathcal{Z} = \mathbb{R}^2$, $\Sigma = \{1,2\}$, $\sigma = 1$ denoting the biplane mode, $\sigma = 2$ denoting the quadcopter mode, $x(t) = \left[V_X(t), V_Z(t)\right]^{\mathrm{T}}$, control input given by $u(t) = \left[\tilde T_X(t), \tilde T_Z(t)\right]^{\mathrm{T}}$, $\Phi_\sigma(t,x) = \left[\theta(t), q(t), \tilde\Phi^{\mathrm{T}}_\sigma(t, x(t))\right]^{\mathrm{T}}$, and $\Theta_{\sigma(t)} = \left[m \begin{bmatrix} -g\cos\theta_{\mathrm{e},\sigma(t)} & 0 \\ -g\sin\theta_{\mathrm{e},\sigma(t)} & a_{3,4,\sigma(t)} \end{bmatrix}, \tilde\Theta^{\mathrm{T}}_{\sigma(t)} \right]^{\mathrm{T}}$. The resetting events for the outer loop, which determine the transitions between quadcopter and biplane modes, can be reduced to the same form as (22) with $g_{\mathrm{d},1}(t,x) = [x, 2]^{\mathrm{T}}$, $g_{\mathrm{d},2}(t,x) = [x, 1]^{\mathrm{T}}$, and

$$\mathcal{R}_\sigma \triangleq \left\{(t,x) \in [t_0,\infty) \times \mathcal{Z} : |\alpha(t)| = \alpha_{\mathrm{stall}}\right\}, \qquad \sigma \in \Sigma. \tag{77}$$

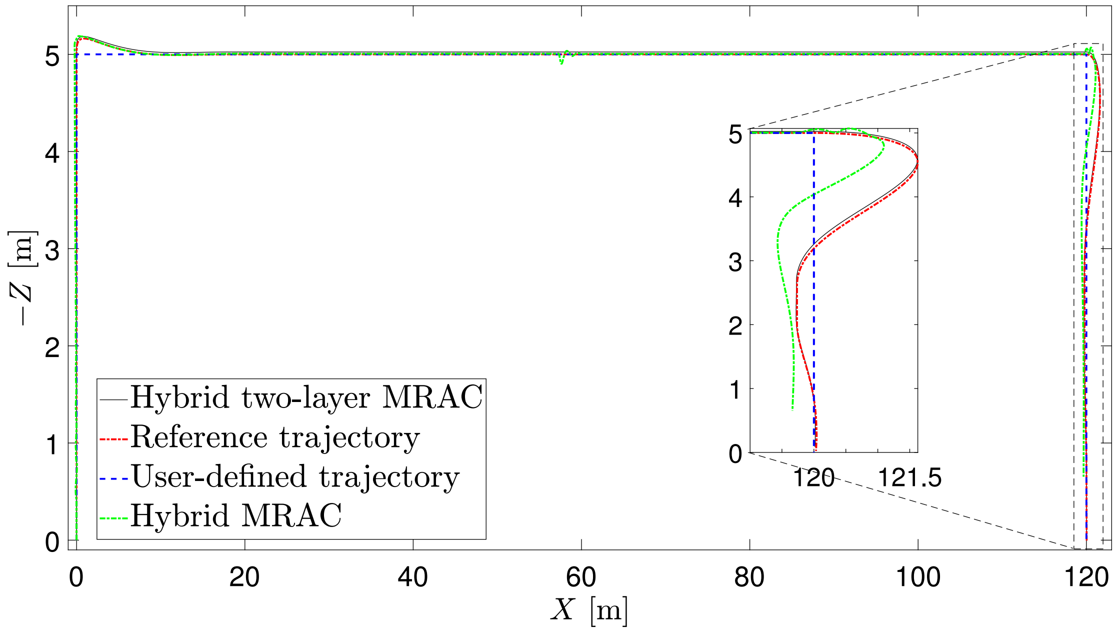

Fig. 6.2. Path followed by the quad-biplane employing the proposed control framework, reference path produced by (24) and (25), user-defined path, and path followed by the quad-biplane employing the results in [4]. Within the given time interval of 60 s, the proposed controller allows the QRBP to follow the user-defined path, whereas the framework presented in [4] requires a longer time interval to complete its mission.

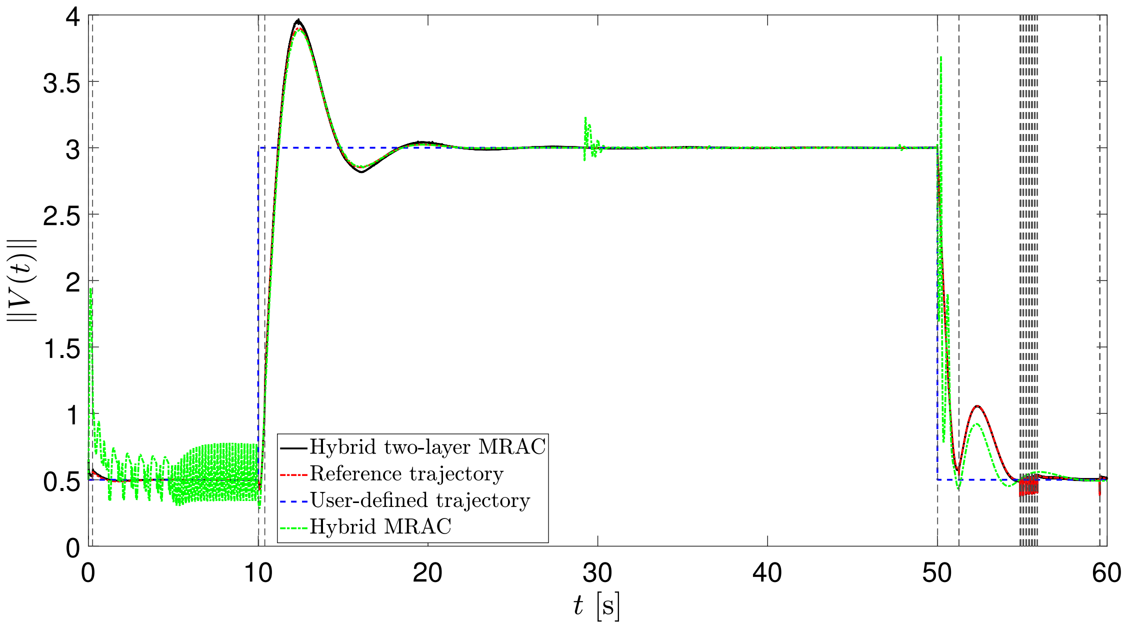

Fig. 6.3. Norm of the translational velocity of a quad-biplane applying the proposed two-layer MRAC framework for NTVH systems and applying the results in [4]. The norm of the velocity of the reference model and the norm of the user-defined velocity are shown as well. The proposed control framework allows following the reference velocity profile more closely than the framework in [4]. Furthermore, the proposed framework does not produce the same high-frequency oscillations as the control framework in [4]. Vertical dotted lines mark the transitions between quadcopter and biplane modes applying the proposed framework.

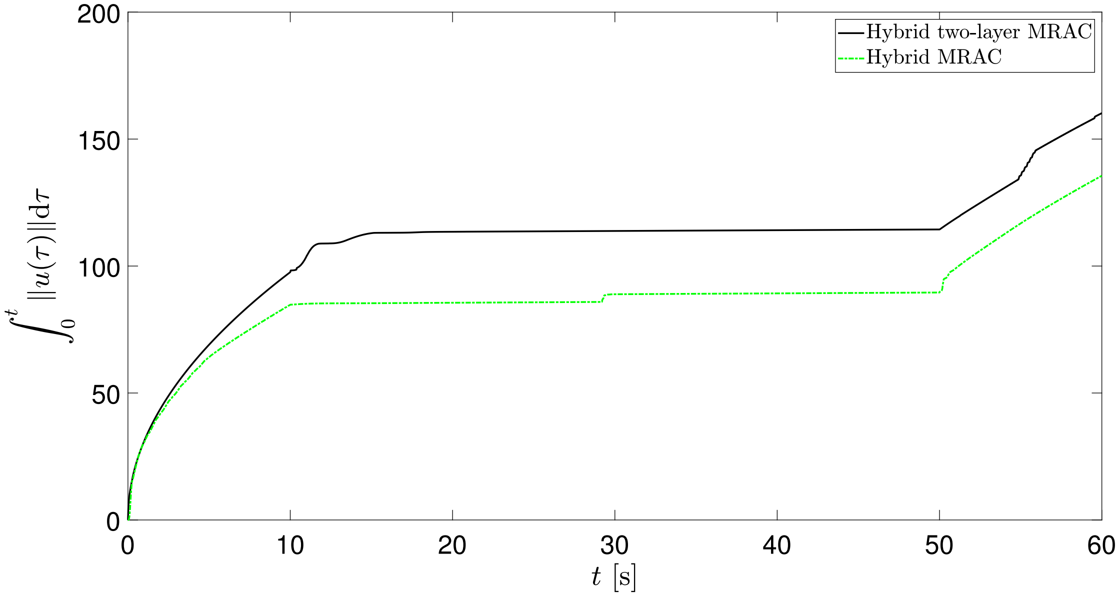

Fig. 6.4. $\mathcal{L}_2$-norm of the control input applying the proposed two-layer MRAC framework for NTVH systems and applying the results in [4]. The proposed system requires a larger, yet comparable, control effort than the framework shown in [4]. Over the time interval $[0, 2.28]$ s circa, the two control efforts are substantially identical, and, after 15.05 s, the difference between the $\mathcal{L}_2$-norm of the control effort employing the proposed approach and employing [4] remains is slightly decreasing.

The reference model for (76) is given by

$$\begin{bmatrix}\dot V_{X,\mathrm{ref}}(t)\\ \dot V_{Z,\mathrm{ref}}(t)\end{bmatrix} = A_{\mathrm{ref,outer}}\begin{bmatrix}V_{X,\mathrm{ref}}(t)\\ V_{Z,\mathrm{ref}}(t)\end{bmatrix} + \begin{bmatrix}\ddot p_{X,\mathrm{user}}(t)\\ \ddot p_{Z,\mathrm{user}}(t)\end{bmatrix} - A_{\mathrm{ref,outer}}\begin{bmatrix}\dot p_{X,\mathrm{user}}(t)\\ \dot p_{Z,\mathrm{user}}(t)\end{bmatrix}$$
$$- A_{\mathrm{ref,outer},2}\left(\int_0^t \begin{bmatrix}V_{X,\mathrm{ref}}(\tau)\\ V_{Z,\mathrm{ref}}(\tau)\end{bmatrix}\mathrm{d}\tau - \begin{bmatrix}p_{X,\mathrm{user}}(t)\\ p_{Z,\mathrm{user}}(t)\end{bmatrix}\right),$$
$$\begin{bmatrix}V_{X,\mathrm{ref}}(t_0)\\ V_{Z,\mathrm{ref}}(t_0)\end{bmatrix} = \begin{bmatrix}\dot p_{X,\mathrm{user}}(t_0)\\ \dot p_{Z,\mathrm{user}}(t_0)\end{bmatrix}, \qquad t \geq t_0, \tag{78}$$

where $A_{\mathrm{ref,outer}}, A_{\mathrm{ref,outer},2} \in \mathbb{R}^{2\times 2}$ are user-defined and Hurwitz, and $[p_{X,\mathrm{user}}, p_{Z,\mathrm{user}}]^{\mathrm{T}} : [t_0, \infty) \to \mathbb{R}^2$ denotes the user-defined, twice continuously differentiable position. The reference model (78) is in the same form as (24) with $x_{\mathrm{ref}}(t) = [V_{X,\mathrm{ref}}(t), V_{Z,\mathrm{ref}}(t)]^{\mathrm{T}}$, $t \geq t_0$, $A_{\mathrm{ref},\sigma} = A_{\mathrm{ref,outer}}$, $B_{\mathrm{ref},\sigma} = \mathbf{1}_2$, and

$$r(t) = \begin{bmatrix}\ddot p_{X,\mathrm{user}}(t)\\ \ddot p_{Z,\mathrm{user}}(t)\end{bmatrix} - A_{\mathrm{ref,outer}}\begin{bmatrix}\dot p_{X,\mathrm{user}}(t)\\ \dot p_{Z,\mathrm{user}}(t)\end{bmatrix} - A_{\mathrm{ref,outer},2}\left(\int_0^t \begin{bmatrix}V_{X,\mathrm{ref}}(\tau)\\ V_{Z,\mathrm{ref}}(\tau)\end{bmatrix}\mathrm{d}\tau - \begin{bmatrix}p_{X,\mathrm{user}}(t)\\ p_{Z,\mathrm{user}}(t)\end{bmatrix}\right).$$

Simulation Results

Figs. 6.2–6.4 show simulation results with $m = 2$ kg, $\bar c = 0.01$ m, $S = 0.5$ m^2, $\rho = 1.225$ kg/m^3, $C_{\mathrm{D},0} = 0.002$, $g = 9.81$ m/s^2, $I_y = 0.01$ kg m^2, $\Gamma_x = \Gamma_r = 2\cdot 10^2 \cdot \mathbf{1}_2$, $\Gamma_\Theta = 10^2\cdot\mathbf{1}_4$, $Q_\sigma = \mathbf{1}_2$, $A_{\mathrm{ref},\sigma} = \begin{bmatrix}-1 & 0\\ 0 & -2\end{bmatrix}$, $\theta_{\mathrm{e},1} = 7°$, $\theta_{\mathrm{e},2} = 90°$, $\alpha_{\mathrm{stall}} = 10°$, and $A_{\mathrm{tran},\sigma} = \begin{bmatrix}-4 & 0\\ 0 & -3\end{bmatrix}$. Fig. 6.2 shows the UAV's path applying the proposed control framework, the control framework in [4], the reference path obtained by the reference model (24) and (25), and the user-defined path. The reference path is unfeasible since it involves to 90° turns at non-zero speed. Applying the same tunable parameters, the proposed control system allows the vehicle to follow the reference path more closely than the control system in [4]. Furthermore, within the given time interval $[0, 60]$ s, the proposed control system allows the UAV to complete its mission, whereas the control system in [4] require additional time to allow the quad-biplane to land. Fig. 6.3 shows the norm of the UAV velocity applying the proposed control framework and the control framework in [4]. The norm of the reference velocity and of the user-defined velocity profile are shown as well. Applying the same tunable parameters, the control system in [4] induces oscillations in the UAV's velocity profile at considerably higher frequencies than the proposed control system. Fig. 6.4 shows the control effort required by the proposed architecture and the architecture in [4]. The proposed system requires a larger, yet comparable, control effort for a higher trajectory tracking performance.

6.2. Control of a disk within a maze

In the following, we consider the problem of controlling a disk tasked with following a user-defined trajectory, while remaining within a confined space; see Figs. 6.5 and 6.9. The walls of this space, which resemble a maze, are impenetrable and, whenever the disk hits these walls, it bounces according to a perfectly elastic model. The user-defined trajectory is ill-designed and penetrates the walls of the maze. Furthermore, the user-defined trajectory requires the disk to perform 90° turns at a non-zero translational velocity. A force applied to the center of the disk serves as control input.

Problem Formulation

Let $p : [t_0, \infty) \to \mathbb{R}^2$ denote the position of the center of the disk, $v(t) \triangleq \dot{p}(t)$ the velocity of the center of mass of the disk, $u : [t_0, \infty) \to \mathbb{R}^2$ the thrust force acting on the disk, $m > 0$ the mass of the disk, $S > 0$ the cross-section area of the disk, $C_{\rm D} > 0$ the drag coefficient of the disk, and $\rho > 0$ the density of the air. According to Newton's law, the continuous-time dynamics of the disk, which captures the motion of the disk between two consecutive bounces against walls, are given by

$$\ddot{p}(t) = m^{-1}\left[u(t) - 0.5\rho S C_{\rm D}\|v(t)\|v(t)\right], \qquad \begin{bmatrix} p(0) \\ \dot{p}(0) \end{bmatrix} = \begin{bmatrix} p_0 \\ v_0 \end{bmatrix}, \qquad t \geq t_0, \tag{79}$$

which is in the same form as (21) with $n = 4$, $m = 2$, $N = 1$, $\mathcal{Z} = \mathbb{R}^4$, $\Sigma = \{1\}$, $x(t) = \left[p^{\rm T}(t), v^{\rm T}(t)\right]^{\rm T}$, $A_\sigma = \begin{bmatrix} 0_{2\times 2} & \mathbf{1}_2 \\ {}_{2\times 2} & {}_{2\times 2} \end{bmatrix}$, $\sigma \in \Sigma$, $B_\sigma = \begin{bmatrix} 0_{2\times 2} \\ m^{-1}\mathbf{1}_2 \end{bmatrix}$, $\tilde{\Phi}_\sigma(t, x) = \|v\|v$, $(t, x) \in [t_0, \infty) \times \mathbb{R}^4$, and $\tilde{\Theta}_\sigma = 0.5\rho S C_{\rm D}\,[1, 1]^{\rm T}$.

To capture the elastic bounce of the disk against hard surfaces, including corners, let $\beta \in [0, 2\pi)$ denote the angle between the horizontal direction and the radial direction of the disk, that is, the direction of the line intersecting both the center of the disk and the point of impact. The translational velocity of the center of the disk before the impact, expressed in the radial and tangential directions, is given by

$$\begin{bmatrix} v_{\rm r}(t) \\ v_{\rm t}(t) \end{bmatrix} = \begin{bmatrix} \cos\beta(t) & \sin\beta(t) \\ -\sin\beta(t) & \cos\beta(t) \end{bmatrix} v(t), \qquad t \in [t_0, \infty). \tag{80}$$

The translational velocity of the center of the disk after the impact, expressed in the radial and tangential coordinates, is given by

$$\begin{bmatrix} v_{\rm r}(t^+) \\ v_{\rm t}(t^+) \end{bmatrix} = \begin{bmatrix} -1 & 0 \\ 0 & 1 \end{bmatrix} \begin{bmatrix} v_{\rm r}(t) \\ v_{\rm t}(t) \end{bmatrix}, \qquad t \in [t_0, \infty). \tag{81}$$

Similarly to (80), the translational velocity of the center of the disk after the impact, expressed in the global coordinates, is given by

$$v(t^+) = \begin{bmatrix} \cos\beta(t) & -\sin\beta(t) \\ \sin\beta(t) & \cos\beta(t) \end{bmatrix} \begin{bmatrix} v_{\rm r}(t^+) \\ v_{\rm t}(t^+) \end{bmatrix}, \qquad t \in [t_0, \infty). \tag{82}$$

Thus, substituting (80) and (81) into (82), we obtain that the disk's discrete-time dynamics across its uncontrolled resetting events, namely bounces against walls, are given by

$$v(t^+) = \begin{bmatrix} -1 + 2\sin^2\beta(t) & -\sin(2\beta(t)) \\ -\sin(2\beta(t)) & \cos(2\beta(t)) \end{bmatrix} v(t), \qquad t \in [t_0, \infty). \tag{83}$$

The resetting event model captured by (83) is in the same form as (22) with $g_{{\rm d},\sigma} = \left[v^{\rm T}(t^+), 1\right]^{\rm T}$, $\sigma \in \Sigma = \{1\}$, $\mathcal{R}_\sigma = [t_0, \infty) \times \{r \in \mathbb{R}^3 : {\rm dist}(r, \mathcal{M}) = R\}$, ${\rm dist}(\cdot, \cdot)$ denoting the Euclidean distance, $\mathcal{M}$ denoting the walls of the maze, and $R > 0$ denoting the radius of the disk.

Given the user-defined trajectory to be followed by the disk $p_{\rm user} : [t_0, \infty) \to \mathbb{R}^2$, to apply the MRAC framework, we consider a reference model that captures the dynamics of a disk not subject to any aerodynamic force and striving to follow the user-defined trajectory. Specifically, we consider a reference model, whose continuous-time dynamics are captured by (24) with $A_{{\rm ref},\sigma} = \begin{bmatrix} 0_{2\times 2} & \mathbf{1}_2 \\ -K_{\rm P} & -K_{\rm D} \end{bmatrix}$, $\sigma \in \Sigma$, where $K_{\rm P}, K_{\rm D} \in \mathbb{R}^{2\times 2}$ are positive-definite, $B_{{\rm ref},\sigma} = \begin{bmatrix} 0_{2\times 2} \\ \mathbf{1}_2 \end{bmatrix}$, and $r(t) = K_{\rm P} p_{\rm user}(t) + K_{\rm D}\dot{p}_{\rm user}(t)$, $t \in [t_0, \infty)$. This way, between resetting events, the state of the reference model $x_{\rm ref}(\cdot)$ is steered toward $\left[p_{\rm user}^{\rm T}(\cdot), \dot{p}_{\rm user}^{\rm T}(\cdot)\right]^{\rm T}$.

Mission Scenario 1 – Simulation Results

The first mission scenario involves the maze and the user-defined trajectory shown in Fig. 6.5. Fig. 6.5 also shows the trajectory of the disk and the reference trajectory. Employing the proposed two-layer MRAC system, the disk closely follows the reference trajectory, compatibly with the hard constraints given by the walls.

The reference trajectory experiences multiple instantaneous variations induced by the resetting events (52) and (53), which aid the plant's trajectory in its task of following the user-defined trajectory, while reducing the tracking error. Employing the control architecture presented in [4], the disk follows the reference trajectory less closely, and the reference trajectory undergoes fewer resetting events and smaller variations across these events. Furthermore, as it can be seen by the disk trajectory after it has avoided the second obstacle, which is represented by the green square on the right side of Fig. 6.5, the disk trajectory reaches the reference trajectory later than it does by applying the proposed framework. Finally, employing the classical MRAC approach, the closed-loop system's tracking performance is further degraded.

Fig. 6.6 shows the position tracking error employing the proposed architecture, the results presented in [4], and classical MRAC. Employing classical MRAC, the position tracking error experiences the largest variations. The proposed approach provides tracking errors that are smaller than those provided by applying the results presented in [4] and classical MRAC for most of the time.

Fig. 6.7 shows the $\mathcal{L}_2$-norm of the velocity tracking errors employing the proposed architecture, the results presented in [4], and classical MRAC. The $\mathcal{L}_2$-norm is employed instead of the classical Euclidean norm because, due to the numerous elastic collisions of

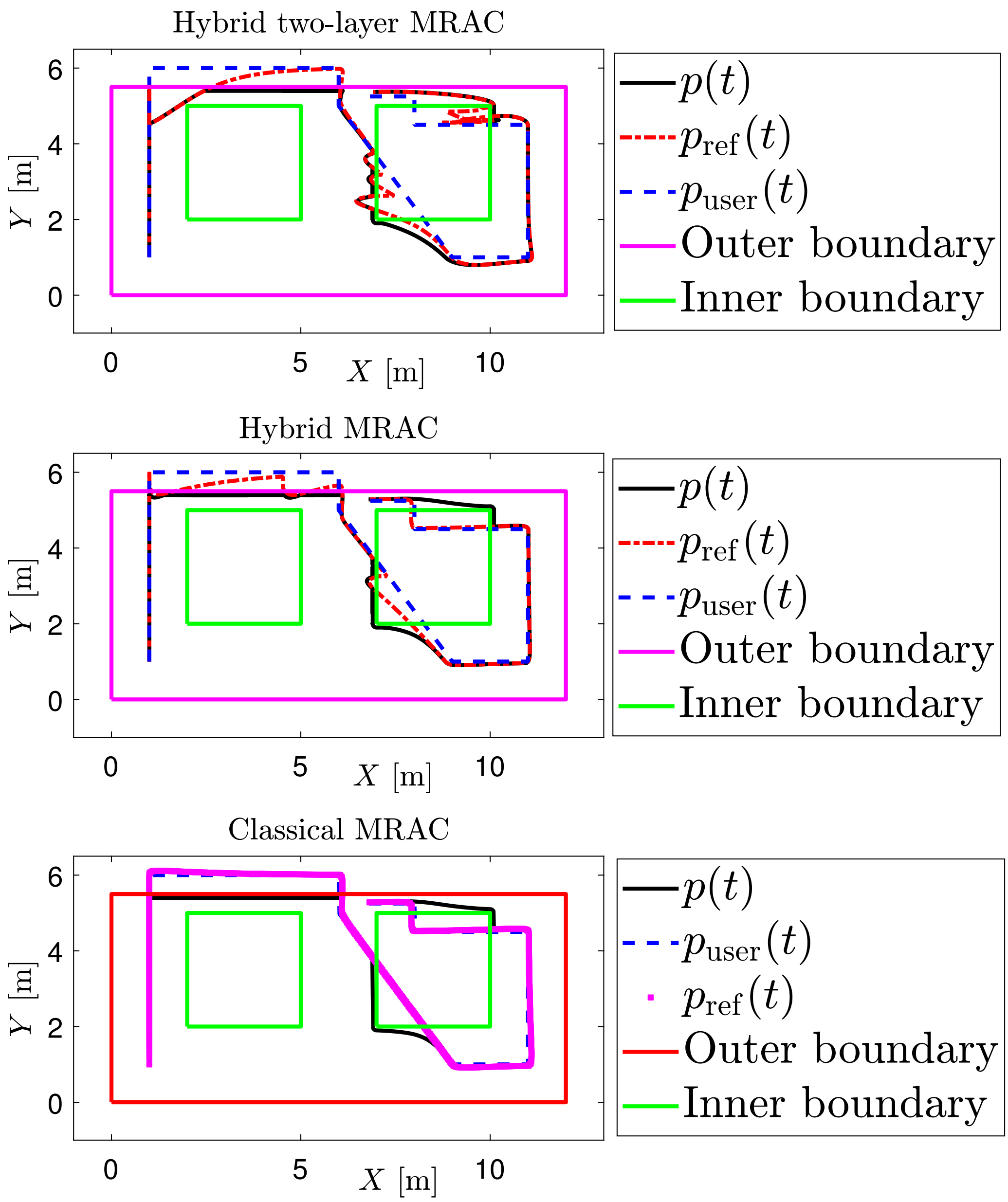

Fig. 6.5. Trajectory of the disk, reference trajectory, and user-defined trajectory obtained by applying the proposed control architecture for NTVH systems, the MRAC architecture for hybrid systems presented in [4], and the classical MRAC architecture. Applying the proposed framework, the disk trajectory converges to the reference trajectory more rapidly, and the reference trajectory undergoes several resetting events that lower the tracking error, while the disk strives to follows the user-defined trajectory and repeatedly bounces against the walls.

the disk against the wall, the Euclidean norm of the velocity tracking error oscillates numerous times at high frequencies. From this figure, it is apparent how the proposed approach guarantees the smallest cumulative velocity tracking error and faster convergence to zero.

Fig. 6.8 shows the control effort employing the three control architectures considered in this analysis. It is apparent how the proposed control architecture guarantees the least control effort. Classical MRAC suffers from the largest variations in the $\mathcal{L}_2$-norm of the control input after 45 s, that is, when the reference trajectory lies within the right square obstacle; see Fig. 6.5.

Mission Scenario 2 – Simulation Results

This mission scenarios has been designed to show that the proposed control framework allows not only for smaller tracking errors and control efforts, but also allows to address practical problems not solvable employing the architecture presented in [4] or

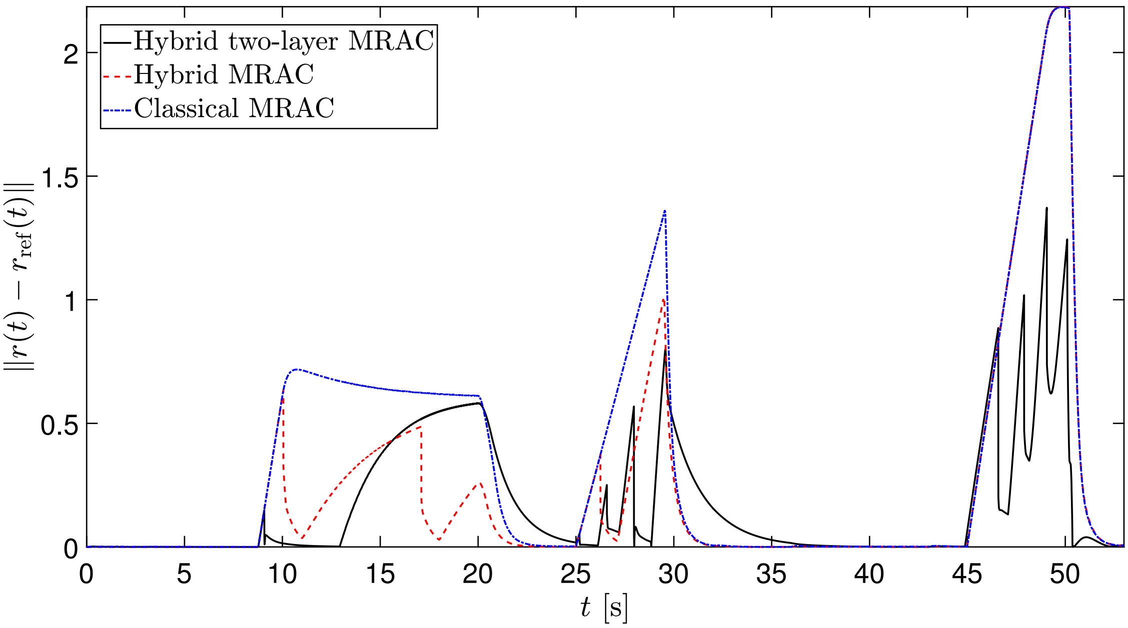

Fig. 6.6. Norm of the position tracking error employing the proposed two-layer MRAC architecture for NTVH systems, the MRAC architecture for hybrid systems presented in [4], and the classical MRAC architecture. The position tracking error is substantially larger and experiences larger variations employing classical MRAC. Furthermore, although both MRAC techniques for hybrid systems show similar values for the tracking error, the proposed control system allows for a faster decay of the tracking error to zero.

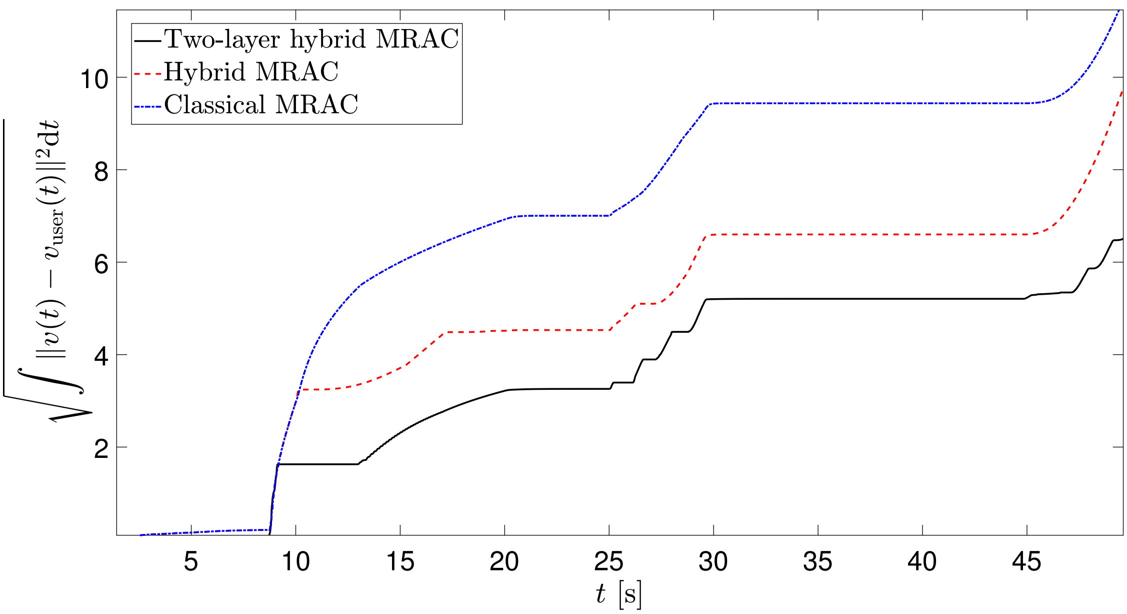

Fig. 6.7. $\mathcal{L}_2$-norm of the position tracking error employing the proposed two-layer MRAC architecture for NTVH systems, the MRAC architecture for hybrid systems presented in [4], and the classical MRAC architecture. Applying the proposed architecture, the velocity tracking error is consistently smaller. The $\mathcal{L}_2$-norm is employed instead of the classical Euclidean norm because, due to the numerous elastic collisions of the disk against the wall, this metric oscillates numerous times at high frequencies.

classical MRAC. In this mission scenario, we add a third obstacle to the maze shown in Fig. 6.9. This obstacle is shown in the third subplot of Fig. 6.9.

As shown in Fig. 6.9, only applying the proposed framework, the disk is able to move away from the corner introduced by the third obstacle, whereas the alternative two techniques considered in this section do not allow such a result. The control system deduced from [4] does not introduce a sufficiently large variation in the reference model to allow the disk to complete its mission;

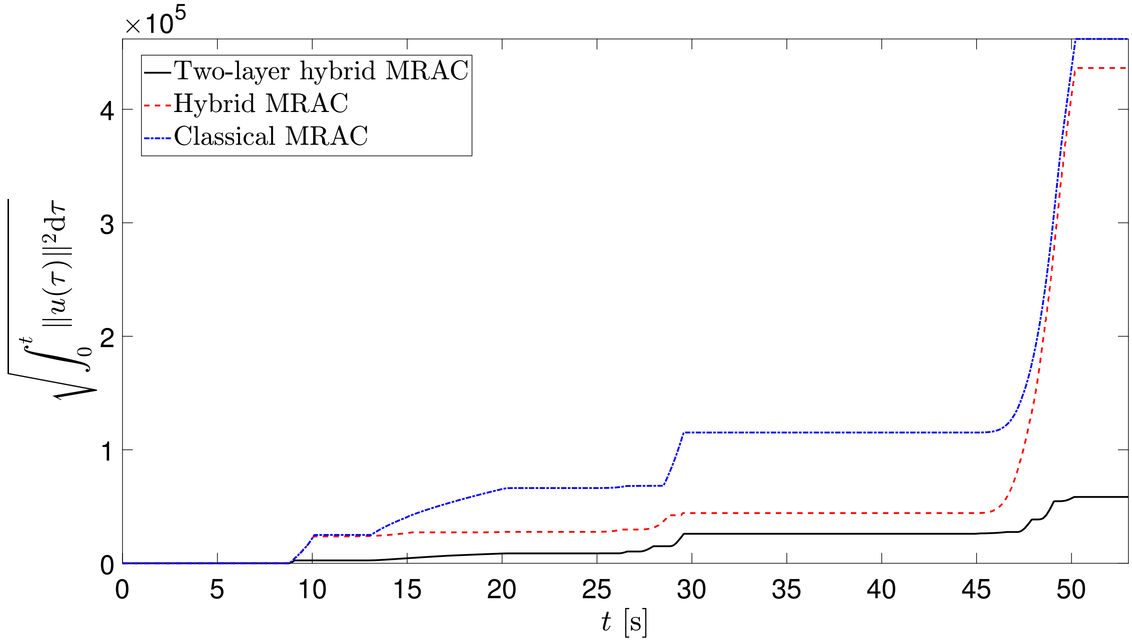

Fig. 6.8. $\mathcal{L}_2$-norm of the control input employing the proposed two-layer MRAC architecture for NTVH systems, the MRAC architecture for hybrid systems presented in [4], and the classical MRAC architecture. Applying the proposed architecture, the control effort is consistently smaller.

a similar unsatisfactory result is obtained by employing the classical MRAC architecture. Furthermore, applying the control system proposed in [4] and the classical MRAC architecture, only when the user-defined trajectory, and, hence, the reference trajectory, are about the reach the end point, which is behind the position where the disk is stuck, the disk manages to trace back its position and reach its final position. A video showing the results of this second simulation scenario are shown in [36].

6.3. Controlling a multi-rotor UAV transporting unsteady payload

We conclude this section with an extensive application involving the designing of the control system of an X8-copter, that is, a UAV equipped with four pairs of counter-rotating propellers. This vehicle is tasked with following an aggressive user-defined trajectory while transporting two unknown steel balls free to move in their casing. The controller is unaware of the presence of the payload, whose impacts on the UAV casing is comparable to that of impulses on the UAV dynamics. In [37], this control problem has already been solved applying the MRAC framework for NHTV systems devised in [4]. In the following, we discuss how the MRAC system proposed in this paper provides improved performances over [4,37].

The control architecture for an X8-copter tasked with aggressive maneuvers is somewhat complex, and is outlined in detail in [37]. In the following, we present key elements of this architecture, namely the vehicle's outer and inner loop dynamics to appreciate how the theoretical framework presented in this paper can be applied to this control problem. Additional details can be found in [37].

Problem Formulation

Since an X8-copter is characterized by six degrees of freedom, namely the position of its center of mass and the Euler angles to capture the UAV's attitude, and four control inputs, namely the total thrust and the three component of the moment of the thrust, the control architecture must comprise an outer loop and an inner loop [3]. The outer loop dynamics are captured by

$$\dot{x}_{\rm tran}(t) = Ax_{\rm tran}(t) + B_{{\rm tran},\sigma}\Lambda_{\sigma(t)}\left[T_{\rm trust,ideal}(t) + \Theta^{\rm T}_{{\rm tran},\sigma(t)}\Phi_{{\rm tran},\sigma(t)}(t, x_{\rm tran}(t))\right],$$
$$x_{\rm tran}(t_0) = \begin{bmatrix} r^{\mathbb{I}}_{A,0} \\ v^{\mathbb{I}}_{A,0}\end{bmatrix}, \qquad t \geq t_0, \tag{84}$$

where $x_{\rm tran}(t) \triangleq \left[r_A^{\rm T}(t), v_A^{\rm T}(t)\right]^{\rm T}$, $r_A : [t_0,\infty) \to \mathbb{R}^3$ denotes the position of the UAV's center of mass, $v_A(t) \triangleq \dot{r}_A(t)$, $A = \begin{bmatrix} 0_{3\times3} & \mathbf{1}_3 \\ 0_{3\times3} & 0_{3\times3}\end{bmatrix}$, $B_{{\rm tran},\sigma} = \begin{bmatrix} 0_{3\times3} \\ \mathbf{1}_3\end{bmatrix}$, $\Lambda_\sigma = m_\sigma^{-1}\mathbf{1}_3$, $m_\sigma > 0$ denotes the mass of the UAV,

$$\Theta_{{\rm tran},\sigma} \triangleq \left[-\frac{1}{2}\rho S_\sigma c_{{\rm D},\sigma}, m_\sigma g \mathbf{1}_3\right]^{\rm T}, \qquad \sigma \in \Sigma, \tag{85}$$

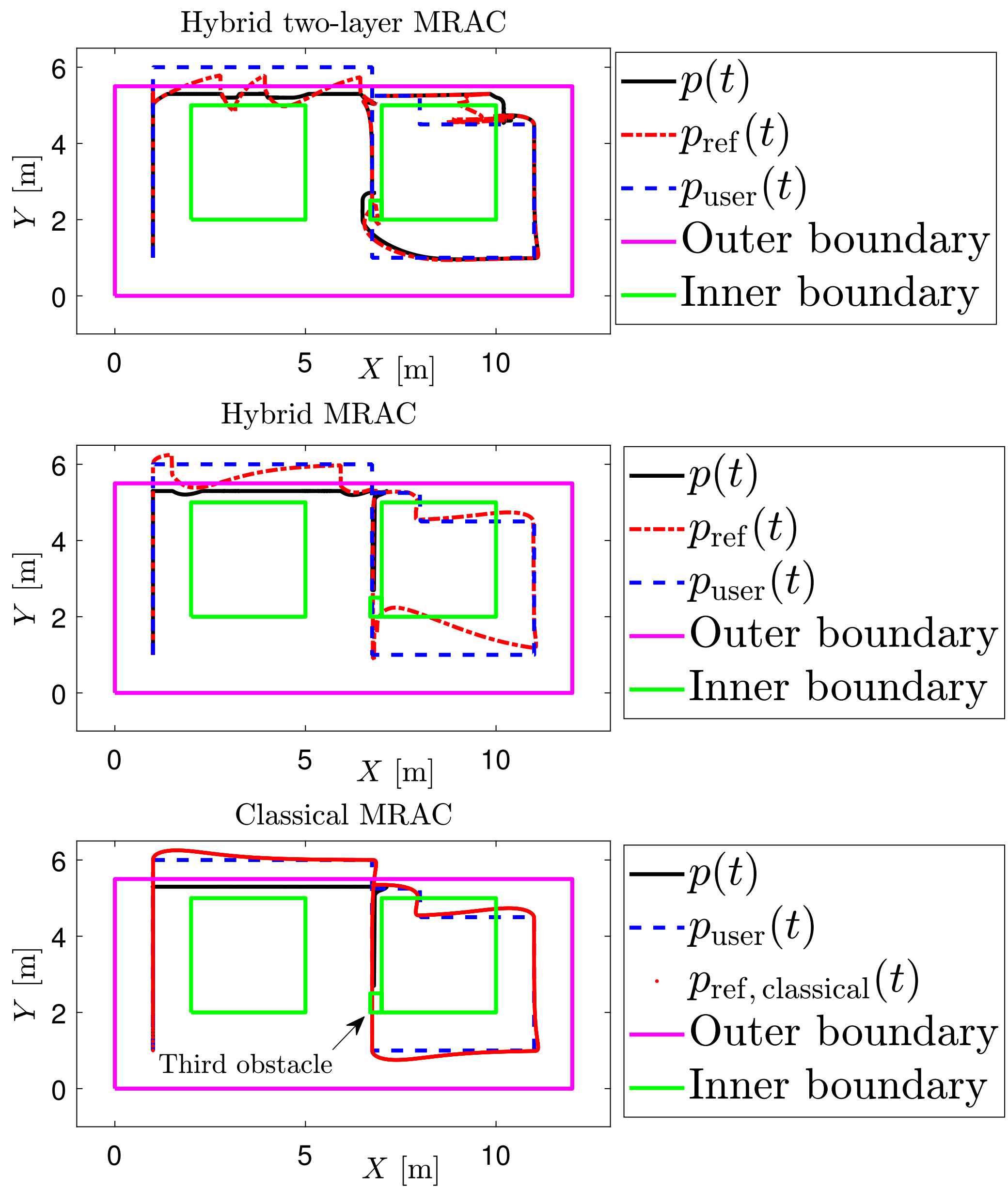

Fig. 6.9. Mission scenario similar to the one presented in Fig. 6.5 with the addition of a third obstacle inside the maze. Applying the results shown in [4] and the classical MRAC framework, this additional obstacle prevents the disk from following the reference trajectory, until the reference trajectory is substantially behind the position, where the disk is stuck. The proposed framework, instead, allows sufficiently large, instantaneous variations in the reference model to let the disk circumnavigate the third obstacle and follow both the reference trajectory and, hence, the user-defined trajectory. A video of showing these simulation results is available at [36].

$$\Phi_{{\rm tran},\sigma}(t,x_{\rm tran}) \triangleq \begin{bmatrix} \|v_A\| R(\phi(t),\theta(t),\psi(t)) v_A \\ e_3 \end{bmatrix}, \qquad (t,x_{\rm tran}) \in [t_0,\infty)\times\mathbb{R}^6, \tag{86}$$

$\rho > 0$ denotes the air density, $S_\sigma > 0$ denotes the reference area cross-section, $c_{{\rm D},\sigma} > 0$ denotes the aerodynamic coefficient, $g > 0$ denotes the gravitational acceleration,

$$R(\phi,\theta,\psi) \triangleq \begin{bmatrix} \cos\psi & -\sin\psi & 0 \\ \sin\psi & \cos\psi & 0 \\ 0 & 0 & 1 \end{bmatrix} \begin{bmatrix} \cos\theta & 0 & \sin\theta \\ 0 & 1 & 0 \\ -\sin\theta & 0 & \cos\theta \end{bmatrix} \begin{bmatrix} 1 & 0 & 0 \\ 0 & \cos\phi & -\sin\phi \\ 0 & \sin\phi & \cos\phi \end{bmatrix},$$
$$(\phi,\theta,\psi) \in [0,2\pi)\times\left(-\frac{\pi}{2},\frac{\pi}{2}\right)\times[0,2\pi), \tag{87}$$

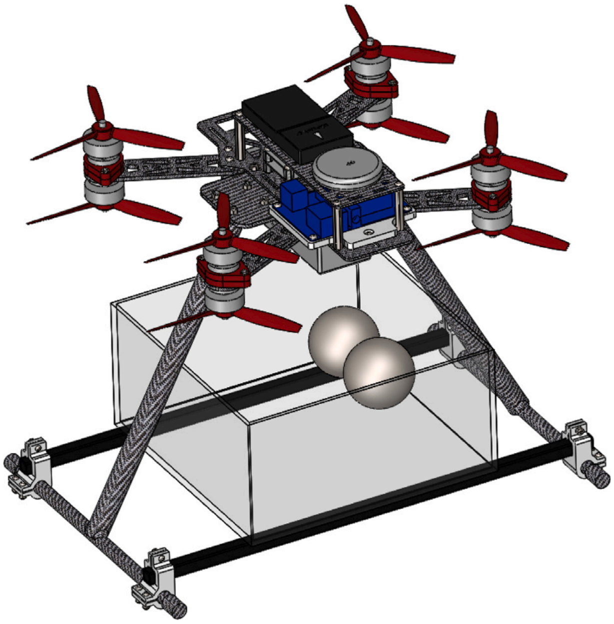

Fig. 6.10. CAD (computer-aided design) representation of an X8-copter transporting two balls, which are free to move within their casing.

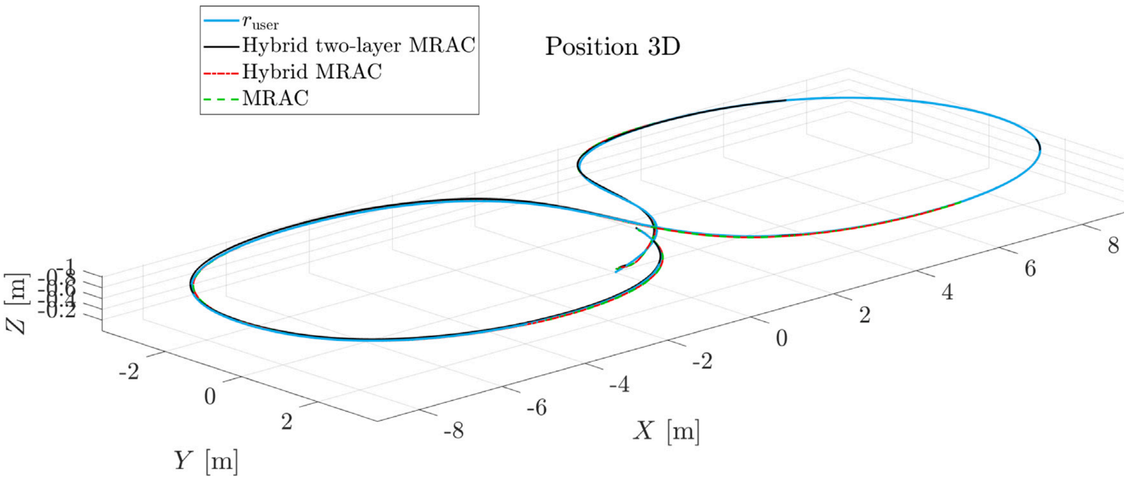

Fig. 6.11. Paths followed by an X8-copter obtained by applying the proposed two-layer MRAC system for NHTV plants, the MRAC system for NHTV plants proposed in [4], and a classical MRAC framework [7, Ch. 9]. It is apparent that, irrespectively of the control system being applied, the UAV's path is closely to the user-defined lemniscate path.

$\phi(\cdot)$ denotes the *roll angle*, $\theta(\cdot)$ denotes the *pitch angle*, $\psi(\cdot)$ denotes the *yaw angle*, and $e_3 \triangleq [0,0,1]^{\mathrm{T}}$. The control input $T_{\text{trust,ideal}} : [t_0,\infty) \to \mathbb{R}^3$ denotes the force needed to steer the UAV along some user-defined trajectory, should the thrust force be pointed at will. The dynamical model (84) is in the same form as (21) with $n = 6$, $m = 4$, $N = 6$, $\mathcal{Z} = \mathbb{R}^6$, $\Sigma = \{1\}$, $x(t) = x_{\text{tran}}(t)$, $u(t) = T_{\text{trust,ideal}}(t)$, $A_\sigma = A$, $\sigma \in \Sigma$, $B_\sigma = \begin{bmatrix} 0_{3\times 3} \\ \mathbf{1}_3 \end{bmatrix}$, $\tilde{\boldsymbol{\Phi}}_\sigma(t,x) = \boldsymbol{\Phi}_{\text{tran},\sigma}(t,x_{\text{tran}})$, $(t,x) \in [t_0,\infty)\times\mathbb{R}^4$, and $\tilde{\Theta}_\sigma = \Theta_{\text{tran},\sigma}$. Remarkably, (84) involves the unknown, diagonal, positive-definite matrix Λ_σ, $\sigma \in \Sigma$, which is not employed in the proposed formulation of two-layer MRAC for NHTV systems; this term poses an additional challenge to the proposed architecture.

The inner loop dynamics are captured by

$$\dot{\omega}(t) = I_{\sigma(t)}^{-1}\left[M_{\text{thrust}}(t) + \Theta_{\text{rot},\sigma}^{\mathrm{T}}\boldsymbol{\Phi}_{\text{rot},\sigma}(t,\omega)\right], \qquad \omega(t_0) = \omega_0, \qquad t \geq t_0, \tag{88}$$

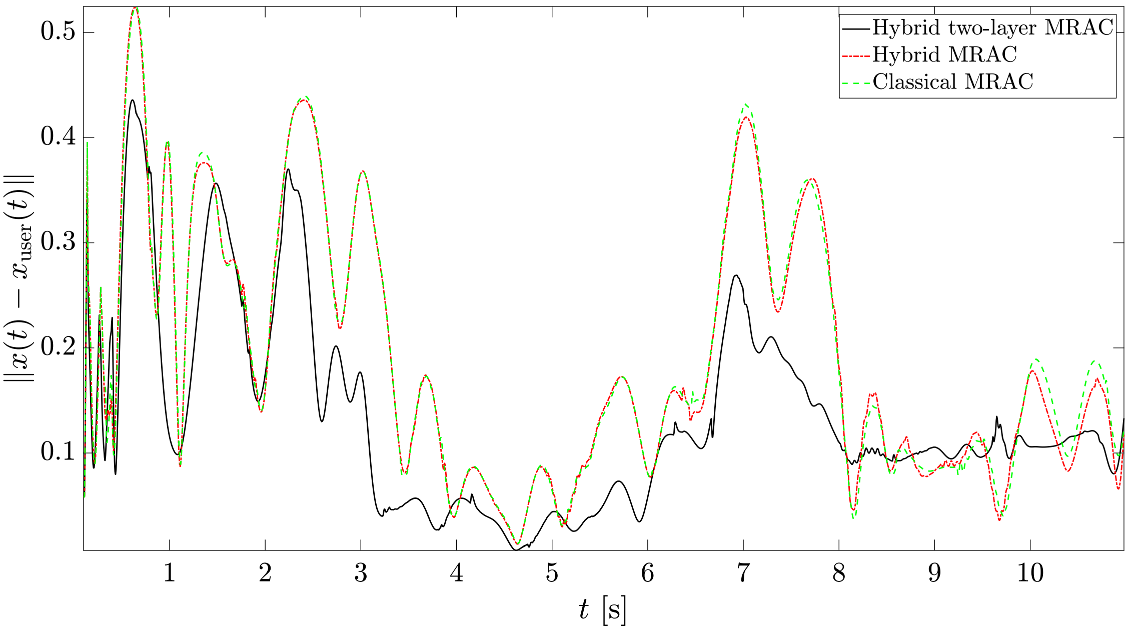

Fig. 6.12. Error in following a user-defined trajectory obtained by applying the proposed two-layer MRAC system for NHTV plants, the MRAC system for NHTV plants proposed in [4], and a classical MRAC framework [7, Ch. 9]. It is apparent how the proposed approach consistently allows for a smaller tracking error than the other techniques.

where, for each $\sigma \in \Sigma$,

$$\Theta_{\text{rot},\sigma} \triangleq \left[-\frac{1}{2}\rho S_\sigma \delta^\times c_{\text{D},\sigma}, \text{diag}\left(\left[I_{zz}-I_{yy}, I_{xx}-I_{zz}, I_{yy}-I_{xx}\right]^{\text{T}}\right)\right]^{\text{T}}, \tag{89}$$

$$\Phi_{\text{rot},\sigma}(t,\omega) \triangleq \begin{bmatrix} \|v_A(t)\| R(\phi(t),\theta(t),\psi(t)) v_A(t) \\ \omega_y\omega_z \\ \omega_x\omega_z \\ \omega_x\omega_y \end{bmatrix}, \qquad (t,\omega) \in [t_0,\infty)\times\mathbb{R}^3, \tag{90}$$

$\omega = \left[\omega_x, \omega_y, \omega_z\right]^{\text{T}}$, $I_\sigma = \text{diag}\left(\left[I_{xx,\sigma}, I_{yy,\sigma}, I_{zz,\sigma}\right]^{\text{T}}\right)$, diag : $\mathbb{R}^n \to \mathbb{R}^{n\times n}$ produces a diagonal matrix from its vector argument, and $\delta \in \mathbb{R}^3$ captures the distance from the center of mass of the UAV and its aerodynamic center, and it is unknown. The dynamical model (88) is in the same form as (21) with $n = 6$, $m = 4$, $N = 6$, $\mathcal{Z} = \mathbb{R}^6$, $\Sigma = \{1\}$, $x(t) = \omega(t)$, $u(t) = T_{\text{trust,ideal}}(t)$, $A_\sigma = 0_{3\times3}$, $\sigma \in \Sigma$, $B_\sigma = \mathbf{1}_3$, $\tilde{\Phi}_\sigma(t,x) = \Phi_{\text{rot},\sigma}(t,\omega)$, and $\tilde{\Theta}_\sigma = \Theta_{\text{rot},\sigma}$. The reference models for (84) and (88) are omitted for brevity and can be designed employing, for instance, proportional-integral controllers to let the reference trajectories follow user-defined profiles; for details, see [37].

Simulation Results

To highlight the advantages of the proposed control system for NHTV systems, we consider the problem of controlling an X8-copter to follow a user-defined three-dimensional lemniscate trajectory at a forward velocity, whose maximum is as high as 7.35 m/s; see Fig. 6.11. To obtain high-fidelity simulation results, the proposed control system has been tested in the PyChrono environment [38]. This software package relieves users from modeling and coding rigid body systems' dynamics. The system dynamics are simulated by applying forces and moments to CAD (computer-aided design) models of the system provided by the user; see Fig. 6.10 for a representation of the CAD model employed in this example. In the context of the proposed simulations, PyChrono allows simulating the interactions between the payload and its casing as well as the gyroscopic and inertial counter-torque effects due to the UAV propellers and its unsteady payload.

In the proposed simulations, we consider a UAV, whose mass is 2.025 kg, and whose matrix of inertia is $10^{-2}\cdot\text{diag}\left([2.2720, 2.2020, 1.6147]^{\text{T}}\right)$ kg m^2, tasked with transporting two balls, whose mass is 0.539 kg each. As shown in Fig. 6.11, the proposed two-layer MRAC system for NHTV plants, the hybrid MRAC system proposed in [4], and a classical MRAC system allow following the user-defined path. However, as shown in Fig. 6.12, the proposed approach allows for a consistently smaller trajectory tracking error than the other techniques. Furthermore, as shown in Fig. 6.13, this higher trajectory tracking performance is obtained applying a consistently smaller or comparable control effort, which makes the proposed control system more effective.

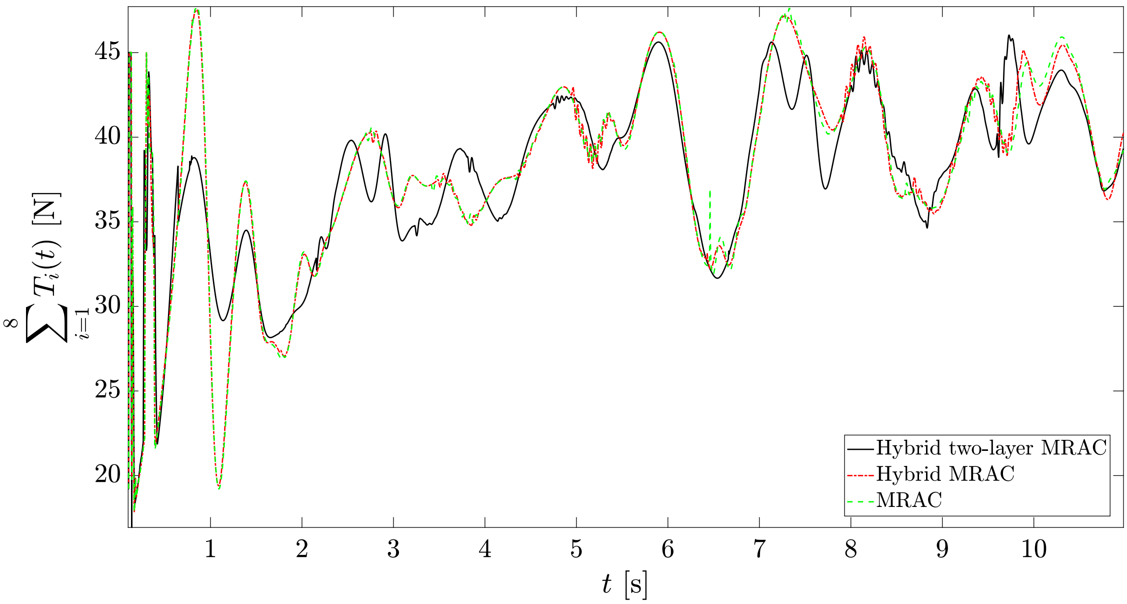

Fig. 6.13. Sum of the thrust forces produced by all propellers required by the proposed two-layer MRAC system for NHTV plants, the MRAC system for NHTV plants proposed in [4], and a classical MRAC framework [7, Ch. 9]. It is apparent how the proposed approach consistently requires a smaller or comparable control effort. In light of the results in Fig. 6.12, the proposed control system provides superior results.

7. Conclusion

This paper proposed an MRAC system for NTVH plants affected by modeling uncertainties in both their continuous time dynamics and their resetting dynamics. For these features, together with the control system presented in [4], this is the only MRAC system able to control this broad class of plants. Despite the results presented in [4], the proposed control system allows to set user-defined rates of convergence across resetting events, and, hence, considerably improved performance. Finally, leveraging a secondary reference model, the proposed control architecture is unique for its ability to set the trajectory tracking error to zero at user-defined, isolated time instants, and preserve the overall closed-loop system's tracking performance.

Numerical evidence show that the proposed framework produces smaller tracking errors for comparable or smaller efforts. The proposed control system allows to address more efficiently control problems, wherein the reference trajectories violate hard constraints, without relying on assumptions on the velocity of the closed-loop trajectory such as those discussed in [39].

Future work directions involve the extension of the proposed framework to plants, whose state is not available for measurement, but only some output function can be leveraged. Additionally, future works will involve the robustification of the proposed techniques.

CRediT authorship contribution statement

Mattia Gramuglia: Software, Validation, Visualization, Writing – original draft, Writing – review & editing, Investigation, Data curation. **Giri M. Kumar:** Software, Validation, Visualization, Writing – original draft, Writing – review & editing. **Andrea L'Afflitto:** Conceptualization, Formal analysis, Funding acquisition, Investigation, Methodology, Project administration, Writing – original draft, Writing – review & editing.

Declaration of competing interest

The authors declare that they have no known competing financial interests or personal relationships that could have appeared to influence the work reported in this paper.

Acknowledgments

This research was in part performed with the support of NSF through the Grant no. 2137159 and the US Army Research Lab under Grant no. W911QX2320001.

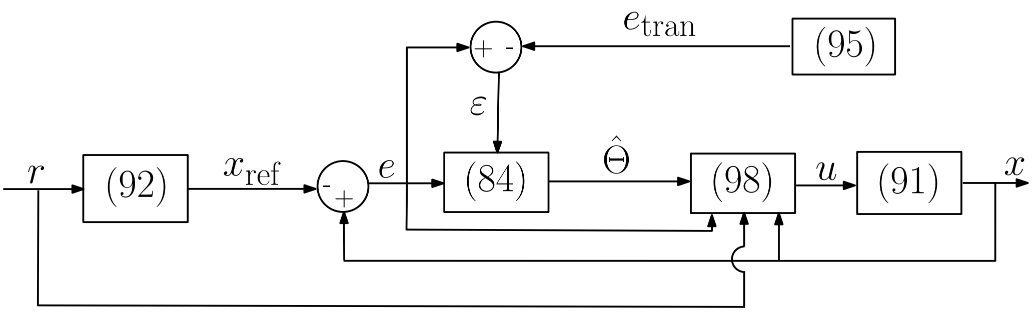

Fig. A.1. Wire diagram of the two-layer MRAC architecture proposed in [8]. It is worthwhile remarking the analogies with the control scheme for NTVH systems shown in Fig. 5.1.

Algorithm 3 Algorithm for two-layer MRAC for continuous-time plants [8]

Input: $x(t)$ ▷ Plant state given by (91)
Output: $u(t)$ ▷ Control input with control law given by (98)
$x_{\text{ref}}(t_0) \leftarrow x_{\text{ref},0}$, $e_{\text{tran}}(t_0) \leftarrow x(t_0) - x_{\text{ref},0}$, $\hat{\Theta}(t_0) \leftarrow \hat{\Theta}_0$ ▷ Set the initial conditions
Set B_{ref}, A_{ref} Hurwitz, & A_{tran} s.t. (96) is verified ▷ Initialize the reference models
while $t \geq t_0$ **do**
  $x_{\text{ref}}(t) \leftarrow \int_{t_0}^{t} \left(A_{\text{ref}} x_{\text{ref}}(t) + B_{\text{ref}} r(t)\right) \mathrm{d}\tau + x_{\text{ref}}(t_0)$ ▷ Apply (92)
  $e_{\text{tran}}(t) \leftarrow \int_{t_0}^{t} A_{\text{tran}} e_{\text{tran}}(\tau) \mathrm{d}\tau + x(t_0) - x_{\text{ref}}(t_0)$ ▷ Apply (95)
  $e(t) \leftarrow x(t) - x_{\text{ref}}(t)$ ▷ Compute the trajectory tracking error
  $\varepsilon(t) \leftarrow e(t) - e_{\text{tran}}(t)$ ▷ Compute the error from the second layer
  $\hat{\Theta}(t) \leftarrow -\int_{t_0}^{t} \Gamma \Phi(t, x(\tau), e(t)) \varepsilon^{\mathrm{T}}(\tau) P B \mathrm{d}\tau + \hat{\Theta}_0$ ▷ Apply (99)
  $u(t) \leftarrow \eta(\hat{\Theta}(t), \Phi(t, x(t), e(t)))$ ▷ Apply (98)
end while

Appendix. Two-layer MRAC for continuous-time systems

In [8], the two-layer MRAC for continuous time systems was presented for the first time. To highlight how the proposed control system for NTVH dynamical systems provides a structure to augment the results in [8], the two-layer MRAC architecture is summarized in the following.

Consider the nonlinear, time-varying plant model affected by parametric and matched uncertainties

$$\dot{x}(t) = Ax(t) + B\left[u(t) + \tilde{\Theta}^{\mathrm{T}} \tilde{\Phi}(t, x(t))\right], \qquad x(t_0), \qquad x_0, \qquad t \geq t_0, \tag{91}$$

where $A \in \mathbb{R}^{n \times n}$ is unknown, $B \in \mathbb{R}^{n \times m}$ is known, $\Theta \in \mathbb{R}^{N \times m}$ is unknown, and $\Phi : [t_0, \infty) \to \mathbb{R}^N$. Furthermore, consider the user-defined reference model

$$\dot{x}_{\text{ref}}(t) = A_{\text{ref}} x(t) + B_{\text{ref}} r(t), \qquad x_{\text{ref}}(t_0), \qquad x_{\text{ref},0}, \qquad t \geq t_0, \tag{92}$$

where $A_{\text{ref}} \in \mathbb{R}^{n \times n}$ is Hurwitz, $B_{\text{ref}} \in \mathbb{R}^{n \times m}$,

$$A_{\text{ref}} = A + BK_x^{\mathrm{T}}, \tag{93}$$

$$B_{\text{ref}} = BK_r^{\mathrm{T}}, \tag{94}$$

for some $K_x \in \mathbb{R}^{n \times m}$ and $K_r \in \mathbb{R}^{m \times m}$, and $r : [t_0, \infty) \to \mathbb{R}^n$ is continuous and bounded. Finally, consider the user-defined auxiliary model

$$\dot{e}_{\text{tran}}(t) = A_{\text{tran}} e_{\text{tran}}(t), \qquad e_{\text{tran}}(t_0) = e_{\text{tran},0}, \qquad t \geq t_0, \tag{95}$$

where $A_{\text{tran}} \in \mathbb{R}^{n \times n}$,

$$\mathrm{Re}\left(\lambda_{\max}\left(A_{\text{tran}}\right)\right) \leq \mathrm{Re}\left(\lambda_{\min}(A_{\text{ref}})\right), \tag{96}$$

and

$$A_{\text{tran}} = A_{\text{ref}} + BK_e^{\mathrm{T}} \tag{97}$$

for some $K_e \in \mathbb{R}^{n \times m}$.

The two-layer MRAC architecture comprises the control law

$$\eta(\hat{\Theta}, \Phi(t, x, e)) = \hat{\Theta}^{\mathrm{T}} \Phi(t, x, e), \qquad (\sigma, t, x, e, \hat{\Theta}) \in [t_0, \infty) \times \mathbb{R}^n \times \mathbb{R}^n \times \mathbb{R}^{\tilde{N} \times m}, \tag{98}$$

where $\Phi(t, x, e) \triangleq \left[x^{\mathrm{T}}, r^{\mathrm{T}}(t), -\tilde{\Phi}^{\mathrm{T}}(t, x), e^{\mathrm{T}}\right]^{\mathrm{T}}$, $e(t) \triangleq x(t) - x_{\mathrm{ref}}(t)$,

$$\dot{\hat{\Theta}}(t) = -\Gamma \Phi(t, x(t), e(t)) \varepsilon^{\mathrm{T}}(t) P B, \qquad \hat{\Theta}(t_0) = \hat{\Theta}_0, \qquad t \geq t_0, \tag{99}$$

denotes the adaptive law $\varepsilon(t) \triangleq e(t) - e_{\mathrm{tran}}(t)$, the user-defined adaptive rate matrix $\Gamma \in \mathbb{R}^{N \times N}$ is symmetric and positive-definite, $N \triangleq n + m + \tilde{N}$, and $P \in \mathbb{R}^{n \times n}$ denotes the symmetric, positive-definite solution of

$$0 = A_{\mathrm{ref}}^{\mathrm{T}} P + P A_{\mathrm{ref}} + Q \tag{100}$$

with $Q \in \mathbb{R}^{n \times n}$ user-defined, symmetric, and positive-definite. This control architecture is summarized by Fig. A.1 and Algorithm 3.

References

[1] H.K. Khalil, Nonlinear Systems, Prentice Hall, Princeton, NJ, 2002.
[2] H. Lin, P. Antsaklis, Hybrid Dynamical Systems: Fundamentals and Methods, Springer, London, UK, 2021.
[3] J.A. Marshall, W. Sun, A. L'Afflitto, A survey of guidance, navigation, and control systems for autonomous multi-rotor small unmanned aerial systems, Annu. Rev. Control 52 (2021) 390–427.
[4] A. L'Afflitto, Model reference adaptive control for nonlinear time-varying hybrid dynamical systems, Internat. J. Adapt. Control Signal Process. 37 (8) (2023) 2162–2183.
[5] W.M. Haddad, V. Chellaboina, Nonlinear Dynamical Systems and Control: A Lyapunov-Based Approach, Princeton Univ. Press, Princeton, NJ, 2008.
[6] R. Goebel, R. Sanfelice, A. Teel, Hybrid Dynamical Systems: Modeling, Stability, and Robustness, Princeton University Press, 2012.
[7] E. Lavretsky, K. Wise, Robust and Adaptive Control: With Aerospace Applications, Springer, London, UK, 2012.
[8] R.B. Anderson, J.A. Marshall, A. L'Afflitto, Novel model reference adaptive control laws for improved transient dynamics and guaranteed saturation constraints, J. Franklin Inst. 358 (12) (2021) 6281–6308.
[9] J. Yang, Y. Liu, J. Na, G. Gao, Improving transient performance of modified model reference adaptive control, in: Q. Zhu, J. Na, X. Wu (Eds.), Innovative Techniques and Applications of Modelling, Identification and Control, Springer, Singapore, 2018, pp. 331–343.
[10] A. L'Afflitto, Barrier Lyapunov functions and constrained model reference adaptive control, IEEE Control Syst. Lett. 2 (3) (2018) 441–446.
[11] J. Yang, J. Na, G. Gao, Robust adaptive control with a modified controller for transient response improvement, in: International Conference on Modelling, Identification and Control, 2017, pp. 929–934.
[12] M. Maghenem, A. Saoud, A. Loria, Adaptive control/identification for hybrid systems part I: With bounded discrete regressor, in: American Control Conference, IEEE, 2022, pp. 3911–3916.
[13] W.M. Haddad, T. Hayakawa, S.G. Nersesov, V. Chellaboina, Hybrid adaptive control for non-linear uncertain impulsive dynamical systems, Internat. J. Adapt. Control Signal Process. 19 (6) (2005) 445–469.
[14] A. Saoud, M. Maghenem, R.G. Sanfelice, A hybrid gradient algorithm for linear regression with hybrid signals, in: American Control Conference, 2021, pp. 4997–5002.
[15] M. De La Sen, Adaptive control of single-input single-output hybrid systems possessing interacting discrete- and continuous-time dynamics, Discrete Dyn. Nat. Soc. 2005 (3) (2005) 299–329.
[16] J. Fu, Z. Ma, Y. Fu, T. Chai, Hybrid adaptive control of nonlinear systems with non-Lipschitz nonlinearities, Systems Control Lett. 156 (2021) 105012.
[17] D. Yang, G. Zong, S.-F. Su, H_∞ tracking control of uncertain Markovian hybrid switching systems: A fuzzy switching dynamic adaptive control approach, IEEE Trans. Cybern. 52 (5) (2022) 3111–3122.
[18] D. Yang, G. Zong, Y. Shi, P. Shi, Adaptive tracking control of hybrid switching Markovian systems with its applications, SIAM J. Control Optim. 61 (2) (2023) 434–457.
[19] M. Maghenem, A. Saoud, A. Loria, Adaptive control/identification for hybrid systems, part II: With linear-growth-order discrete regressor, in: American Control Conference, IEEE, 2022, pp. 3917–3922.
[20] R.B. Anderson, J.A. Marshall, A. L'Afflitto, J.M. Dotterweich, Model reference adaptive control of switched dynamical systems with applications to aerial robotics, J. Intell. Robot. Syst. 100 (3) (2020) 1265–1281.
[21] M. di Bernardo, U. Montanaro, S. Santini, Hybrid model reference adaptive control of piecewise affine systems, IEEE Trans. Automat. Control 58 (2) (2013) 304–316.
[22] M. di Bernardo, U. Montanaro, R. Ortega, S. Santini, Extended hybrid model reference adaptive control of piecewise affine systems, Nonlinear Anal.: Hybrid Syst. 21 (2016) 11–21.
[23] S. Kersting, M. Buss, Direct and indirect model reference adaptive control for multivariable piecewise affine systems, IEEE Trans. Automat. Control 62 (11) (2017) 5634–5649.
[24] D.S. Bernstein, Matrix Mathematics: Theory, Facts, and Formulas, Second Edition, Princeton University Press, Princeton, NJ, 2009.
[25] W.M. Haddad, V.S. Chellaboina, S.G. Nersesov, Impulsive and Hybrid Dynamical Systems: Stability, Dissipativity, and Control, Princeton, Princeton, NJ, 2014.
[26] R.G. Sanfelice, R. Goebel, A.R. Teel, Generalized solutions to hybrid dynamical systems, Control Optim. Calc. Var. 14 (4) (2008) 699–724.
[27] M. Bardi, I. Capuzzo-Dolcetta, Optimal Control and Viscosity Solutions of Hamilton–Jacobi–Bellman Equations, Birkhäuser, Boston, MA, 2008.
[28] F.H. Clarke, Optimization and Nonsmooth Analysis, Society of Industrial and Applied Mathematics, Philadelphia, PA, 1989.
[29] S. Boyd, L. El Ghaoui, E. Feron, V. Balakrishnan, Linear Matrix Inequalities in System and Control Theory, SIAM, Philadelphia, PA, 1994.
[30] P.J. Antsaklis, A.N. Michel, A Linear Systems Primer, Birkhäuser, Boston, MA, 2007.
[31] B. Kågström, Bounds and perturbation bounds for the matrix exponential, IEEE Trans. Biomed. Eng. 17 (1) (2015) 39–57.
[32] I.M. Mareels, B.D. Anderson, R.R. Bitmead, M. Bodson, S.S. Sastry, Revisiting the MIT rule for adaptive control, in: IFAC Proceedings Volumes, Vol. 20, 1987, pp. 161–166, (2).
[33] A. L'Afflitto, A Mathematical Perspective on Flight Dynamics and Control, Springer, London, UK, 2017.
[34] S. Swarnkar, H. Parwana, M. Kothari, A. Abhishek, Biplane-quadrotor tail-sitter UAV: Flight dynamics and control, J. Guid. Control Dyn. 41 (5) (2018) 1049–1067.
[35] J.A. Marshall, G.I. Carter, A. L'Afflitto, Model reference adaptive control for prescribed performance and longitudinal control of a tail-sitter UAV, in: SciTech Forum, AIAA, San Diego, CA, pp. 1–16.
[36] M. Gramuglia, G.M. Kumar, A. L'Afflitto, Two-layer model reference adaptive control for uncertain hybrid dynamical systems, 2023, https://youtu.be/NuBNfV1NWXk. Last accessed 07/10/2023.

[37] M. Gramuglia, G.M. Kumar, A. L'Afflitto, A hybrid model reference adaptive control system for multi-rotor unmanned aerial vehicles, in: SciTech, AIAA, Orlando, FL, 2024, pp. 1–21.
[38] A. Tasora, R. Serban, H. Mazhar, A. Pazouki, D. Melanz, J. Fleischmann, M. Taylor, H. Sugiyama, D. Negrut, Chrono: An open source multi-physics dynamics engine, in: T. Kozubek (Ed.), High Performance Computing in Science and Engineering, Springer, 2016, pp. 19–49.
[39] A. L'Afflitto, T.A. Blackford, Constrained dynamical systems, robust model reference adaptive control, and unreliable reference signals, Internat. J. Control 93 (5) (2020) 1039–1052.